Neutrophils Induce Astroglial Differentiation and Migration of Human Neural Stem Cells via C1q and C3a Synthesis

Mitra J. Hooshmand,[*,†,‡] Hal X. Nguyen,[*,†,§,1] Katja M. Piltti,[*,†,‡,1] Francisca Benavente,[*,†,‡,1] Samuel Hong,[¶] Lisa Flanagan,[†] Nobuko Uchida,[‖] Brian J. Cummings,[*,†,‡,§] and Aileen J. Anderson[*,†,‡,§]

Inflammatory processes play a key role in pathophysiology of many neurologic diseases/trauma, but the effect of immune cells and factors on neurotransplantation strategies remains unclear. We hypothesized that cellular and humoral components of innate immunity alter fate and migration of human neural stem cells (hNSC). In these experiments, conditioned media collected from polymorphonuclear leukocytes (PMN) selectively increased hNSC astrogliogenesis and promoted cell migration in vitro. PMN were shown to generate C1q and C3a; exposure of hNSC to PMN-synthesized concentrations of these complement proteins promoted astrogliogenesis and cell migration. Furthermore, in vitro, Abs directed against C1q and C3a reversed the fate and migration effects observed. In a proof-of-concept in vivo experiment, blockade of C1q and C3a transiently altered hNSC migration and reversed astroglial fate after spinal cord injury. Collectively, these data suggest that modulation of the innate/humoral inflammatory microenvironment may impact the potential of cell-based therapies for recovery and repair following CNS pathology. ***The Journal of Immunology*****, 2017, 199: 1069–1085.**

The efficacy of therapeutic neurotransplantation targeting CNS disease/trauma will be heavily dependent on interactions between donor cells and the cellular and molecular microenvironment. The importance of environmental cues for neural stem cell (NSC) properties became clear in early studies demonstrating region-specific fate profiles within the intact CNS (1, 2). Although the CNS has traditionally been considered immune privileged, neuroinflammation is now known to be a hallmark of neurodegeneration/trauma, including activation of innate and adaptive immunity and infiltration of a diverse array of inflammatory cells and molecules (3–7). We hypothesize that cross-talk between NSC and the immune system may be critical for both endogenous and donor cell responses in the injured, diseased, or aged CNS.

The immunomodulatory effects of donor stem cells on the host have been studied extensively, particularly in the case of mesenchymal stem cell populations, but also in the context of NSC populations (8–12). The converse, that is the effect of the host cellular immune response on donor stem cells, has received less attention. T cells, microglia, and their secreted components have been shown to alter the properties of NSC or neural progenitor/precursor cell (NPC) populations (9, 13–17). Both activated microglia and some of their secreted factors such as TNF-α and IL-6 have been previously described to inhibit neuron production both in vitro and in vivo (17, 18). Similarly, cytokines/chemokines and other pro- and anti-inflammatory molecules have been shown to regulate NSC/NPC survival, proliferation, fate, and migration (reviewed in Ref. 19). However, the effect of infiltrating innate immune cells and humoral components of the innate immune response, for example, neutrophils, macrophages (Mϕ), and cytokines/proteins of the complement cascade, on stem cells remains to be elucidated. In particular, expression of complement receptor CR2 by rodent NPC has recently been identified and shown as a regulator of adult neurogenesis (20), and C3a has been shown to modulate ischemia-induced astrocyte survival (21), suggesting that neural and glial cells can interact with components of the complement cascade.

In the current study, we investigated whether factors synthesized by immune cells that infiltrate the CNS acutely after injury could alter the fate and migration of human NSC (hNSC), thereby significantly influencing the therapeutic application of cell therapies in the clinical setting. We show that conditioned media (CM) derived from two distinct populations of immune cells, polymorphonuclear leukocytes (PMN) and Mϕ, alter migration and differentiation of hNSC in vitro. Furthermore, we identify complement components C1q and C3a as molecular mediators for these novel effects. Finally, in a proof-of-concept neurotransplantation experiment, we demonstrate that blockade of C1q and C3a in vivo can alter hNSC fate and migration in the acute phase of spinal cord injury (SCI), when both PMN infiltration and complement activation peak.

*Institute for Memory Impairments and Neurological Disorders, University of California, Irvine, Irvine, CA 92697; [†]Sue and Bill Gross Stem Cell Research Center, University of California, Irvine, Irvine, CA 92697; [‡]Department of Anatomy and Neurobiology, University of California, Irvine, Irvine, CA 92697; [§]Department of Physical Medicine and Rehabilitation, University of California, Irvine, Irvine, CA 92697; [¶]Bridges to Stem Cell Research Program, California State University, Fullerton, Fullerton, CA 92834; and [‖]StemCells Inc., Palo Alto, CA 94304

[1]H.X.N., K.M.P., and F.B. contributed equally to this work.

ORCIDs: 0000-0001-6159-6934 (M.J.H.); 0000-0002-3212-9891 (H.X.N.); 0000-0002-9773-0442 (K.M.P.); 0000-0002-6870-6857 (S.H.); 0000-0003-3628-5290 (B.J.C.).

Received for publication February 1, 2016. Accepted for publication May 31, 2017.

This work was supported by National Institutes of Health Grant NS49885 (to A.J.A.), California Institute for Regenerative Medicine Grant RS1-00377-1 (to B.J.C.), Paralysis Project of America Grant PPA-32574 (to H.X.N.), California Institute for Regenerative Medicine Stem Cell Training Award T1-00008 (to H.X.N.), Christopher and Dana Reeve Foundation Grant CRF-AAC 2005 (to A.J.A.), and StemCells Inc.

Address correspondence and reprint requests to Dr. Mitra J. Hooshmand, Institute for Memory Impairments and Neurological Disorders, University of California, Irvine, 2010 Sue and Bill Gross Hall, Irvine, CA 92697. E-mail address: mitrah@uci.edu

The online version of this article contains supplemental material.

Abbreviations used in this article: CC3, cleaved caspase-3; CE, coefficient of error; CM, conditioned medium; DIV, day in vitro; DM, differentiation medium; ELANE, neutrophil elastase; GFAP, glial fibrillary acidic protein; hNSC, human NSC; KO, knockout; Mϕ, macrophage; NPC, neural progenitor/precursor cell; NSC, neural stem cell; PI, propidium iodide; PMN, polymorphonuclear leukocyte; SCI, spinal cord injury.

Materials and Methods

All procedures involving animals were conducted in accordance with the Institutional Animal Care and Use Committee guidelines at University of California, Irvine.

Generation of PMN or Mϕ-CM

CM was generated from PMN or Mϕ isolated from the peritoneal cavity of NOD-*scid* mice for all experiments, with the exception of the following: 1) Fig. 1H, in which immune-sufficient rats were used to replicate the effects of NOD-*scid*–derived CM on NSC, and 2) Supplemental Fig. 1B, 1C, in which knockout (KO) mice on the BUB/BnJ complement-sufficient background were specifically used to investigate the role of C1q/C3a in PMN-CM. NOD-*scid* mice were selected to enable comparison between in vitro (Figs. 1–8) and in vivo (Figs. 9, 10) data, in which donor human cells were xenografted into the mouse spinal cord. NOD-*scid* mice are T cell and B cell deficient, making this model optimal and widely used for xenotransplantation studies in which the survival of donor human cells is a critical variable (22). Importantly, although NOD-*scid* mice exhibit deficits in adaptive immunity, they demonstrate innate immune responses and histopathological characteristics comparable to other mouse strains following SCI (23).

Briefly, adult female mice received 12% sodium caseinate (i.p.) and were sacrificed 12–16 h later (to obtain PMN) or 3–5 d later (to obtain Mϕ), as described previously (24). The peritoneal exudate containing leukocytes was overlaid on Histopaque 1077 (Sigma-Aldrich) and centrifuged at 400 × *g* to separate PMN (12–16 h postsodium caseinate) or Mϕ (3–5 d postsodium caseinate) from other leukocytes, yielding 97% PMN and 80% F4/80$^+$ Mϕ, respectively. Aliquots of isolated cells were mounted on slides and stained with a mouse anti-PMN Ab (1:500; Serotec), a mouse anti-F4/80 Ab (1:100; Serotec), and hematoxylin to confirm cell populations by nuclear morphology and quantify enrichment.

For CM generation, PMN or Mϕ were incubated in NSC differentiation medium (DM), composed of X-vivo media containing BDNF (10 ng/ml), GDNF (10 ng/ml), ciproflaxacin (10 mg/ml), N2 (1:100), heparin (2 mg/ml), *N*-acetyl-L-cysteine (63 mg/ml), basic fibroblast factor (1 ng/ml), and B27 (1:50) supplement for 24 h. CM was derived using this DM composition to enable comparison with the control condition for NSC, which was DM alone. CM was then recentrifuged twice at 2000 rpm for 2 min and collected for use. The effects of NOD-*scid*–derived CM on NSC were replicated using CM derived from fully immune-sufficient Sprague–Dawley rats, according to the sodium caseinate method described above (Fig. 1H). Viability and survival of PMN and Mϕ in DM were confirmed by flow cytometry, as described below. To test the dose–response relationship between PMN and Mϕ-CM and cell migration (Fig. 4), isolated PMN and Mϕ were seeded at initial densities ranging from 156,000 to 2,500,000 cells/ml in DM and CM collected as above. Based on NSC migration results with these CM (Fig. 4A, 4B), CM used in all other in vitro migration and fate experiments was derived from an initial seeding density of 2,500,000 PMN or Mϕ per milliliter.

PMN viability analysis by flow cytometry

PMN and Mϕ (2,500,000 cells/ml) viability following CM generation from C57BL/6 mice described above was tested using propidium iodide (PI) incorporation that can be quantified by flow cytometry. A total of 2 μl/ml PI (1 mg/ml; Invitrogen) was added to PMN maintained in culture for 24 h under the conditions used to generate CM. After a 15- to 20-min incubation period at 37°C, CM (containing floating PMN) was collected in a 15-ml tube, and adherent PMN were detached with 500 μl TrypLE (Invitrogen). Collected floating or adherent PMN were combined into a single sample, and the combined collected cell pellet was resuspended in 300 μl PBS and analyzed on a BD LSR II flow cytometer; the analyzed cell pellet therefore included both live and dead PMN. As previously described (25), dead cells were quantified by gating to viable cells that did not receive PI. The mean values of PMN-positive cells for PI were expressed as percentage (±SE relative to PMN that did not receive PI treatment). Data are averaged across three separate experiments (n = 3; Fig. 1A, 1B).

hNSC culture, cell fate, cell death, and proliferation analysis

Multipotent hCNS-derived stem cells (referred to as hNSC from this point forward) were isolated from 16 to 20 wk gestation human fetal brain and propagated as neurospheres (StemCells), as described previously (26). Briefly, hNSC are isolated by prospective sorting for a CD133$^+$/CD34$^-$/CD45$^-$/CD24$^{-/lo}$ population (26, 27), which enriches for NSC that exhibit neurosphere-initiating capacity by 2000-fold. Cells derived in this manner retain multipotent capacity for >10 passages in vitro and differentiate in a site-specific manner upon transplantation, generating neurons, oligodendrocytes, and astrocytes.

To assess the effect of PMN and Mϕ-CM or purified C1q and/or C3a, hNSC at passages 9–11 were dissociated into single cells and plated on eight-well chamber slides. For fate analysis, 1 d postplating, DM was changed to either DM control or CM conditions (see Table I for details). For immunocytochemistry, hNSC were fixed with 2% paraformaldehyde at 7 or 14 d in vitro (DIV), permeabilized, and blocked in PBS solution supplemented with 0.1% Triton X-100 (Sigma-Aldrich), 5% goat or donkey serum (Jackson ImmunoResearch), and 1% BSA (Sigma-Aldrich). Primary and secondary Abs (including glial fibrillary acidic protein [GFAP], Olig2, and β-tubulin III), sources, and the dilutions at which they were used are listed in Table II. Hoechst 33342 (1:1000 dilution; Invitrogen) was used as a nuclear counterstain.

Table I. List of conditions used in in vitro fate analysis and chemotactic assay

Condition	Host Species	Concentration or Dilution Used	Manufacturer	Catalogue Number
Purified C1q (C1q[PMN])	Human serum	28 ng/ml	My Biosource	MBS143105
Purified C1q (C1q[Mϕ])	Human serum	400 ng/ml	My Biosource	MBS143105
Purified C3a (C3a[PMN])	Human	18.5 ng/ml	Quidel	Component of kit A015, predecessor to A031
Purified C3a (C3a[Mϕ])	Human	120 ng/ml	Quidel	Component of kit A015, predecessor to A031
Purified C3a desArg	Human	18.5 ng/ml	Complement Technologies	A119
SDF1α	Human	200 ng/ml	PeproTech	300-28A
αC1q	Goat anti-human	20 μg/ml (chemotaxis); 1.65 μg/ml (fate); 100 μg/ml in vivo	Quidel	A301
αC3α	Mouse anti-human	20 μg/ml (chemotaxis); 1.65 μg/ml (fate); 100 μg/ml in vivo	Millipore	CBL191
αTNF-α	Rabbit anti–TNF-α	2 and 6 μg/ml	Millipore	AB2148P
αSDF1α	Mouse anti-SDF1α	100 μg/ml	Millipore	MABC184
C1q IgG control	Goat IgG	20 μg/ml in vitro and 2000 μg/ml in vivo	Jackson ImmunoResearch and R&D Systems	005-000-005
C3a IgG control	Mouse IgG	20 μg/ml in vitro and 2000 μg/ml in vivo	Jackson ImmunoResearch and R&D Systems	015-000-003
LY294002	N/A	50 μM dissolved in DMSO	Life Technologies	PHZ1144
PD98059	N/A	10 μM dissolved in DMSO	Life Technologies	PHZ1164
DMSO	N/A	1:1000	Sigma-Aldrich	D26650

N/A, not available.

Table II. List of Abs used for immunocyto/histochemical analyses and Western blots

Ab	Host	Dilution of Primary Ab (In Vivo)	Dilution of Primary Ab (In Vitro)	Manufacturer of Primary Ab	Specificity of Primary Ab	Secondary Ab (In Vitro and In Vivo)
BrdU	Rat	N/A	1:100	Serotec	Proliferating cells	Alexa Fluor donkey anti-rat Fab fragment 488 (1:5–10,000)
β-Tubulin III	Rabbit	1:5000	1:100	Covance	Neurons	Biotinylated or Alexa Fluor 488–conjugated donkey anti-rabbit Fab fragment (1:5–10,0000)
CC1	Mouse	1:4000	N/A	Calbiochem	Mature oligodendrocytes	Biotinylated donkey anti-mouse Fab fragment (1:10,000)
CC3	Rabbit	N/A	1:100	Cell Signaling Technology	Apoptotic cells	Alexa Fluor donkey anti-rabbit IgG 555 (1:5,000)
Fibronectin	Rabbit	1:500	N/A	Sigma-Aldrich	Fibronectin-containing lesion	Biotinylated donkey anti-rabbit Fab fragment (1:10,000)
GFAP	Rabbit	1:60,000	1:100	Dako	GFAP-positive astrocytes	Biotinylated or Alexa Fluor 555–conjugated donkey anti-rabbit Fab fragment (1:10,000)
Olig-2	Goat	1:100	1:100	R&D Systems	Oligodendrocyte progenitor cells	Biotinylated or Alexa Fluor 488–conjugated donkey anti-goat Fab fragment (1:10,000)
SC121	Mouse	1:3000	N/A	StemCells	Human cytoplasm	Biotinylated donkey anti-mouse Fab fragment (1:10,000)
SC123	Mouse	1:3000	N/A	StemCells	Human-positive astrocytes	Biotinylated donkey anti-mouse Fab fragment (1:10,000)
Sox2	Goat	1:200	N/A	Santa Cruz Biotechnology	Sox2-positive progenitor cells	Alexa Fluor donkey anti-goat 488 (1:200)
GAPDH	Rabbit	1:1000	N/A	Cell Signaling	Housekeeping	ECL donkey anti-mouse Fab fragment (1:10,000)
C3	Goat	1:200	N/A	Quidel	Human and mouse C3	ECL donkey anti-goat IgG, HRP-linked whole Ab (1:10,0000)
C1q	Goat	1:200	N/A	Quidel	Human and mouse C1q	ECL donkey anti-goat IgG, HRP-linked whole Ab (1:10,0000)
β-Actin	Mouse	1:1000	N/A	Sigma-Aldrich	β-actin	ECL donkey anti-mouse IgG, HRP-linked whole Ab (1:10,0000)
p-ERK	Rabbit	1:1000	N/A	Cell Signaling Technology	Phosphorylated ERK	ECL donkey anti-rabbit IgG, HRP-linked whole Ab (1:10,0000)
p-AKT	Rabbit	1:1000	N/A	Cell Signaling Technology	Phosphorylated AKT	ECL donkey anti-rabbit IgG, HRP-linked whole Ab (1:10,0000)

N/A, not applicable.

Fluorescent images of immunostained slides were captured using random sampling on a FluoViewFV10i confocal microscope using a ×20 objective, and saved as red, blue, and green channels. Images were merged and quantified using Volocity 5.0 software (28). For all experiments using hNSC, n = 8–10 images per condition per experiment and a minimum of three independent experiments was analyzed. When cultures were prepared across a specific timeline, all time points in those experiments were run in parallel for staining and quantification. For assessment of cell death and cell proliferation, hNSC were plated in the conditions described above and fixed at 1, 2, 3, or 7 DIV, and

Table III. List of primers

Name of Primer	Forward	Reverse
C3aR	5′-TCGCTGGCTCACTTGGCTCTC-3′	5′-CATCCCTACATTGCGATGATT-3′
gC1qR	5′-AGTGCGGAAAGTTGCCGGGGA-3′	5′-GAGCTCCACCAGCTCATCTGC-3′
SDF1α	5′-CCATGGACGCCAAGGTCGTC-3′	5′-GGGCTGTTGTGCTTACTTGTTT-3′
ELANE	5′-GTGGACACAGTACCGAGGAC-3′	5′-CCAGTTGCTTCGGATGAGGG-3′
Factor B	5′-TTCACCCAGTATGAGGAGTCC-3′	5′-GCTGACCATTGTGGAGACCT-3′
Factor D	5′-CGGATGACGACTCTGTGCAG-3′	5′-TCATACCATCGCTTGTAGGGT-3′
Complement factor properdin	5′-TTCACCCAGTATGAGGAGTCC-3′	5′-GCTGACCATTGTGGAGACCT-3′
GAPDH (human)	5′-TGGAAATCCCATCACCATCT-3′	5′-GTCTTCTGGGTGGCAGTGAT-3′
GAPDH (mouse)	5′-TGACCTCAACTACATGGTCTACA-3′	5′-CTTCCCATTCTCGGCCTTG-3′

GAPDH (human) was used in Supplemental Fig. 3, and GAPDH (mouse) was used in Fig. 5 and Fig. 8F′.

Table IV. Number of animals per group for in vivo studies

Group	Time of Sacrifice	Plane of Section Cut/Purpose	*N*	Exclusions
αC1q Ab + αC3a Ab + hNSC	12 wk posttransplant	Transverse/Fate and lesion quantification	7	$n = 1$ was excluded in fate quantification due to poor immunostaining
αC1q Ab + αC3a Ab + hNSC	12 wk posttransplant	Parasagittal/Histology	2	None
αC1q Ab + αC3a Ab + hNSC	6 wk posttransplant	Parasagittal/Histology	2	None
Vehicle + hNSC	12 wk posttransplant	Transverse/Fate and lesion quantification	5	None
Vehicle + hNSC	6 wk posttransplant	Parasagittal/Histology	5	None
Vehicle + hNSC	12 wk posttransplant	Parasagittal/Histology	2	None

immunocytochemistry was conducted using Abs directed against cleaved caspase-3 (CC3) to assay for cell death, or BrdU (10 μM) to label for BrdU incorporation by proliferating cells (Table II provides list of the Abs). All experiments in which hNSC were used were conducted in biological triplicate or quadruplicate with technical replicates.

Transwell migration assays

hNSC at passages 9–11 were prepared and dissociated as above. Source and concentration of individual proteins, Abs, IgGs, or inhibitors used are indicated in Table I. Single cells were resuspended in DM. One hundred fifty microliters of media for each condition was added to the wells of the feeder tray (Millipore), and 100 μl dissociated hNSC (300,000 cells/ml DM) was added to the migration chambers, followed by incubation for 3.5 h at 37˚C. Migration chambers were removed, placed on new 96-well trays containing 150 μl prewarmed cell detachment buffer in the wells, and incubated for 30 min at 37˚C. At the end of the incubation, 50 μl 1:75 dilution of CyQuant GR Dye:Lysis buffer was added to the cell detachment buffer and incubated for 15 min at room temperature. Finally, 150 μl CyQuant GR Dye:Lysis/detachment solution was transferred to a new 96-well plate, and migration was quantified using a 480/520-nm filter set on a fluorescent plate reader. To obtain fluorescence standardization, cells of known doses, as well as blanks containing cell detachment buffer, lysis buffer, and CyQuant Dye, were used. All experiments were conducted in biological triplicate or quadruplicate with technical replicates.

Blocking Abs

Abs against C1q and C3a, as well as SDF1α and TNF-α, were employed to test the effect and specificity of complement component blockade on hNSC fate and migration at 7 DIV (Table I). Inhibition of C3a-, SDF1α-, and TNF-α–mediated responses by blocking Abs has been a widely used tool. C3a, SDF1α, and TNF-α blocking Abs were selected based on specificity, for example, lack of cross-reactivity with whole C3, and previously established function-blocking activity in vitro and in vivo (29–31). In the case of anti-C3a, although this Ab has been shown to have cross-reactivity with human, guinea pig, and rabbit C3a, cross-reactivity with mouse has not been previously characterized. Finally, although this Ab is a mouse monoclonal, this does not pose a confounding variable because the Ab was used either in vitro or in vivo in immunodeficient NOD-*scid* mice, which lack circulating IgG and IgM.

In contrast, there are no previously characterized assays in which C1q plays a similarly defined role in which function-blocking activity of specific Abs has been assessed. A polyclonal anti-C1q Ab was selected based on wide use in previous studies; specificity for C1q from humans, rats, and mice based on immunoblots; and previous characterization in commercially available human clinical ELISAs and immunoaffinity chromatography (32). In all cases, species- and subtype-matched IgG control Abs were confirmed to lack modifying activity (Table I).

RT-PCR

Expression of mRNA for gC1qR and C3aR by hNSC, and SDF1α, neutrophil elastase (ELANE), complement factor B, complement factor D, and complement factor P (properdin) by PMN was assayed by RT-PCR. GAPDH mRNA was assayed in parallel as a housekeeping standard. Briefly, mRNA from hNSC under nondifferentiating conditions was isolated (RNeasy MiniKit; Qiagen), and RT-PCR was performed (OneStep RT-PCR; Qiagen), as follows: 0.25 μg mRNA per condition; 30 min at 50˚C; 15 min at 95˚C; and 30 repeated cycles of 1 min at 95˚C, 1 min at 55˚C, 1 min at 72˚C, ending with 10 min at 72˚C. For C3aR and gC1qR, human primers were selected to investigate receptor expression by human cells. For SDF1α, ELANE, complement factor B, complement factor D, and complement factor P, mouse primers were selected to investigate mRNA synthesis by PMN derived from mice; mouse liver RNA was included as a positive control to validate SDF1α expression detection by this primer set and lack of expression by PMN. A complete list of all primers used is provided in Table III.

ELISAs and C3 cleavage inhibition

C1q concentration in NOD-*scid* PMN-CM (2,500,000 cells/ml), Mϕ-CM (2,500,000 cells/ml), and DM control media was measured using a human C1q ELISA kit (HK356; Hycult), according to the manufacturer's instructions. This kit is reported by the manufacturer to cross-react with mouse C1q. C3a concentration in NOD-*scid* PMN-CM and DM control media was measured initially using a human C3a ELISA kit (A015; Quidel) that has also been shown to recognize mouse C3a (Fig. 5B, 5D). Prior to completion of all studies for this manuscript, Quidel ceased production of A015 and incorporated a different Ab against human C3a in a new ELISA kit (A031), which did not recognize mouse C3a in our experiments. Accordingly, subsequent studies (Fig. 5F, 5G) were completed using a different C3a ELISA kit (A354; Hycult), which recognizes both mouse and human C3a.

Briefly, PMN were collected from NOD-*scid* mice and plated in DM control, as described above, at 2,500,000 seeding density. To verify active C3 cleavage to C3a, 1 μg/ml C3 or equal volume of DM control was added to cultured PMN, and C3a generation was measured after 24 h of incubation at 37˚C (Fig. 5F). To test the mechanism of C3a generation, EDTA, PMSF, DIFP, or equal volume of DM control was added to cultured PMN, and C3a generation was measured in PMN-CM after 24 h of incubation at 37˚C (Fig. 5G). The effect of Ca^{2+}/Mg^{2+} chelation on C3a generation was tested using 1 and 10 mM EDTA. The effect of serine protease inhibition on C3a generation was tested using 0.1 and 0.5 mM PMSF (catalogue P7626; Sigma-Aldrich) or DIFP (catalogue D0879; Sigma-Aldrich). These experiments were conducted in biological triplicate (Fig. 5F, 5G) or biological duplicate with technical replicates or triplicates (Fig. 5A–D).

p-AKT and p-ERK signaling

To assess the induction of hNSC signaling by PMN-CM, NSC were grown in monolayer at 90% confluence, treated either with PMN-CM derived from 3-mo-old C1q KO and C3 KO BUB/BnJ mice and their littermate controls (wild type) or with purified C1q and C3a at the concentrations measured in CM, referred to as C1q plus C3a[PMN] and C1q plus C3a [Mϕ]. PMN-CM was isolated, as described above. hNSC were lysed in RIPA buffer (Sigma-Aldrich) containing protease and phosphatase inhibitor mixture (cOmplete ULTRA Tablets EASYpack, and PhosSTOP; Roche) immediately (0 s), 30 min, 1 h, or 2 h after PMN-CM addition. Protein concentration was determined in precleared extracts using the micro bicinchoninic acid protein assay (Pierce, Rockford, IL) with BSA as standard. Equal amounts of protein were resolved in SDS-PAGE

Table V. CE values for stereological quantification in vivo

Marker	Group	CE Value
SC121	Vehicle; Ab group	0.04; 0.04
SC123	Vehicle; Ab group	0.10; 0.11
CC1	Vehicle; Ab group	0.12; 0.14
Olig-2	Vehicle; Ab group	0.07; 0.08

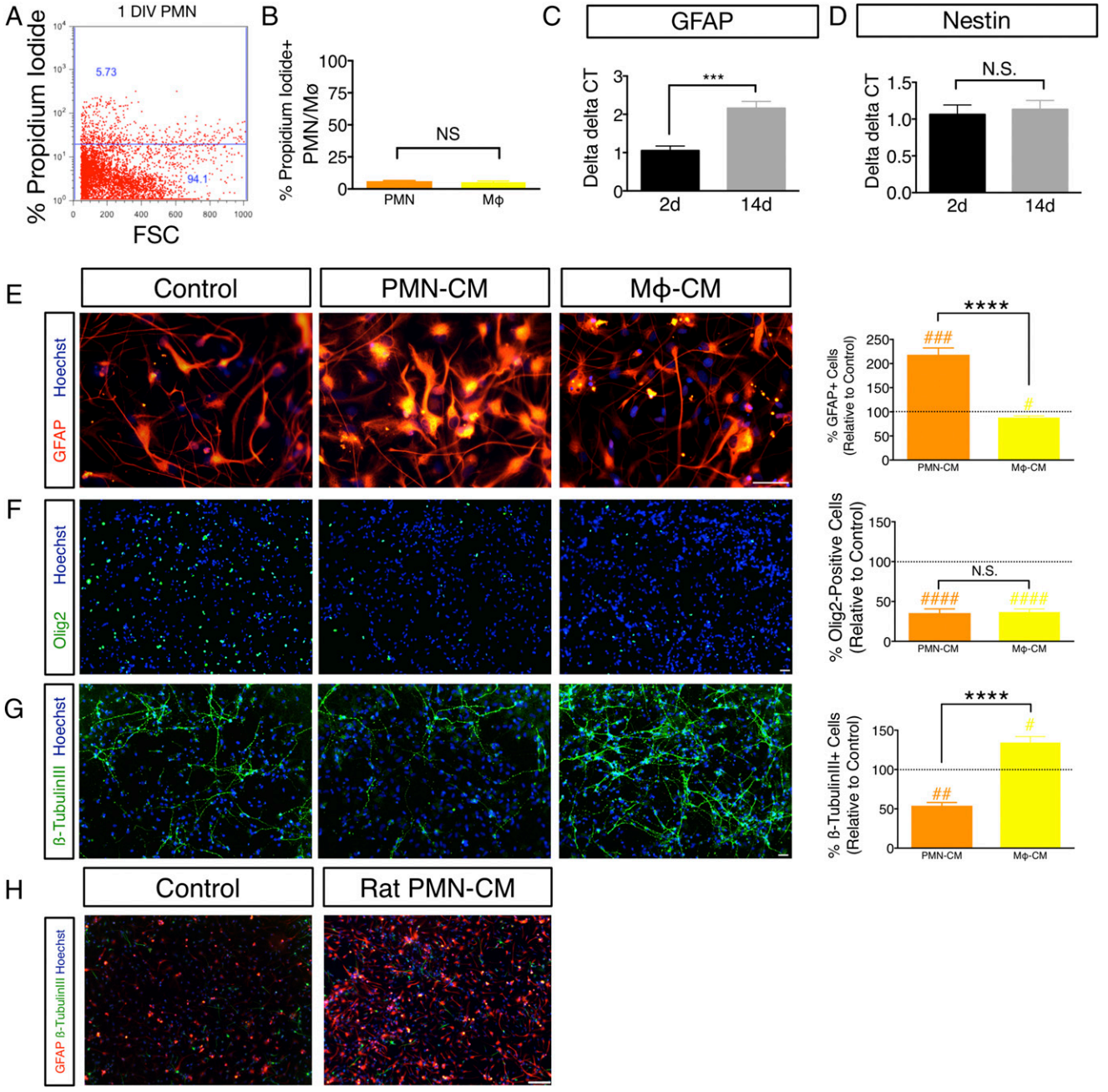

FIGURE 1. PMN-CM promotes astroglial differentiation in vitro. (**A** and **B**) PMN or Mϕ retain viability after 24 h of culture in DM. (A) The number of PI^+ PMN and Mϕ was quantified using flow cytometry, as illustrated for PMN by scatterplot. Dead cells were quantified by gating to viable cells that did not receive PI. (B) Quantification of PI^+ PMN (orange bars) and Mϕ (yellow bars); PMN = 6.04% ± 0.30, Mϕ = 5.27% ± 0.86. Mean percentage ± SEM relative to control IgG or IgM isotype-labeled cells (Student *t* test, $p > 0.05$, N.S.). $n = 3$ technical replicates and $n = 3$ biological replicates/condition. (**C** and **D**) GFAP is a reliable marker for hNSC astroglial lineage commitment under differentiation conditions in vitro. (C) hNSC at passages 9–11 were dissociated into single cells, plated with DM onto eight-well chamber slides (30,000 cells/ml), and maintained at 37°C under standard 5% CO_2 20% O_2 culture conditions for 2 DIV (black bars) or 14 DIV (gray bars) and mRNA collected for quantitative RT-PCR. GFAP mRNA exhibited a 2-fold increase between 2 and 14 DIV under these differentiation conditions (Student *t* test, $^{***}p \leq 0.0001$). $n = 3$ biological replicates/condition. (D) In contrast, Nestin mRNA remained unchanged between 2 and 14 DIV (Student *t* test, $p > 0.05$, N.S.). $n = 3$ biological replicates/condition. (**E**–**G**) hNSC were exposed to either DM (control), or PMN-CM or Mϕ-CM. PMN-CM (orange bars) or Mϕ-CM (yellow bars) versus DM control (dashed line) comparisons were conducted using one-sample *t* tests ($^{\#}p < 0.05$, $^{\#\#}p < 0.01$, $^{\#\#\#}p < 0.001$, $^{\#\#\#\#}p < 0.0001$). Comparisons between groups were performed using one-tailed Student *t* tests ($^{****}p < 0.0001$). (E) PMN-CM increased the percentage of hNSC expressing GFAP compared with control and Mϕ-CM at 14 DIV. (F) PMN-CM and Mϕ-CM reduced the percentage of $Olig2^+$ cells compared with control at 14 DIV, but were not significantly different from each other. (G) PMN-CM reduced the percentage of β-tubulin III^+ cells compared with control and Mϕ-CM at 14 DIV. Mϕ-CM increased the percentage of β-tubulin III expression. $n = 2$ technical replicates and $n = 2$–3 biological replicates/condition. (**H**) PMN-CM derived from immune-sufficient rats promotes astroglial differentiation in vitro. Immunocytochemical staining for GFAP (red), β-tubulin III (green), and Hoechst counterstain (blue) in hNSC exposed to DM control or PMN-CM isolated from the peritoneal cavity of immune-sufficient Sprague–Dawley rats. hNSC treated with PMN-CM exhibited increased $GFAP^+$ cell number in comparison with DM control. Mean ± SEM. Scale bars, 25 μm (E–G) and 150 μm (H).

Table VI. GFAP is a reliable marker for hNSC astroglial lineage commitment under differentiation conditions in vitro

Marker	Percent	SEM, %
$GFAP^+/Sox2^-$	19.35	4.79
$GFAP^+/Sox2^+$	0.284	0.14
$GFAP^-/Sox2^+$	19.15	3.8

hNPCs were cultured for 14 DIV and immunostained for GFAP and Sox2. Quantification of $GFAP^+/Sox2^+$ cell number revealed only 0.28% cells coexpressing these markers after 14 DIV. $n = 3$ images per well; $n = 1$ biological replicate. Mean ± SEM.

precast 4–12% gradient gels (NuPAGE Bis-Tris Gel; Life Technologies, Carlsbad, CA), transferred onto Nitrocellulose Pre-Cut Blotting Membranes NuPAGE (Life Technologies) in a semiwet chamber Trans-Blot SD Semi-Dry Cell (Bio-Rad, Hercules, CA), and subjected to Western blot analysis. Abs against p-AKT, p-ERK, and β-actin were used for immunodetection. Bound Abs were visualized using HRP-coupled secondary Abs anti-mouse and anti-rabbit, followed by detection of labeled proteins using SuperSignal West Dura ECL kit (Pierce) and ChemiDoc imaging system (Bio-Rad). Optical band intensities in each group were normalized to those visualized using anti–β-actin Ab and compared using ImageJ (National Institutes of Health; https://imagej.nih.gov/nih-image/). All Abs, sources, and dilutions are provided in Table II.

Detection of C1q and C3 at the SCI epicenter

Two-month-old female C57BL/6 mice received either a laminectomy (control; $n = 1$) or a moderate contusion injury (50 kilodynes; $n = 1$) at the thoracic level T9, as described below. Twenty-four hours following SCI or laminectomy, the spinal cord was freshly dissected and divided into a 3-mm segment centered at T9, and sequential 3-mm segments extending rostral and caudal from T9. Total protein extraction (RIPA buffer) with protease and phosphatase inhibitors was performed, and complement proteins were analyzed by SDS-PAGE using αC1q- and αC3-specific Abs (C1q Quidel A301; C3 Quidel A304), essentially as described above. GAPDH was used as the loading control in all experiments. Source and dilutions of all Abs are provided under Table II.

Contusion injuries

A total of 22 female NOD-*scid* mice (10 wk old; Jackson Laboratories) was anesthetized using isofluorane and received a laminectomy at the thoracic vertebrae 9 (T9) using a surgical microscope. Animals received 50 kilodyne (1 dyne = 10 μN) contusion injuries using the Infinite Horizon Impactor (Precision Systems and Instrumentation, Lexington, KY), as previously described (33). As noted above, although NOD-*scid* mice exhibit deficits in adaptive immunity, they demonstrate innate immune responses and histopathological characteristics comparable to other mouse strains following SCI (23).

Administration of Abs directed against C1q and C3a in vivo

Immediately after injury, 2 μl either αC1q plus αC3a Abs (100 μg/ml each) or IgG Abs (200 μg/ml) or vehicle were delivered via epicenter injections using a Hamilton Flexifil Syringe over 2 min, followed by a 1-min delay prior to withdrawal of syringe. The effect of αC1q plus αC3a Abs at the concentration delivered in vivo was first tested in vitro, and no toxic or proliferative effects associated with exposure of hNSC to the Abs were observed. Animals were randomly assigned to receive either αC1q plus αC3a Ab with hNSC or vehicle injection (media in which Abs were prepared) with hNSC. Number of animals per group and exclusions are detailed in Table IV.

hNSC transplantation

Neurospheres were dissociated into a single-cell suspension and concentrated to a final density of 75,000 cells/μl injection buffer on the day of SCI, and transplants were conducted, as described previously (33). Briefly, siliconized beveled glass pipettes (bevel: inner diameter = 70 μm, outer diameter = 100–110 μm; Sutter Instruments, Novato, CA) were loaded with freshly triturated hNSC or injection buffer, and injections were made into the intact parenchyma (two sites bilaterally above and below the injury epicenter) at T9 using a NanoInjector system and micropositioner (WPI Instruments, Waltham, MA) immediately after αC1q plus αC3a Abs or vehicle injection. Each site received 250 nl cells or vehicle, delivered in 50 nl vol over 75 s, followed by a 2-min delay before withdrawal of the pipette (34). Previous studies in our laboratory have demonstrated that this volume does not exacerbate damage to the spinal cord.

After the completion of both αC1q plus αC3a Abs or vehicle injection and hNSC transplants, a small piece of gel foam was placed over the site of laminectomy and the musculature was sutured with chromic gut. Animals received lactated ringers (50 ml/kg) s.c. immediately after surgery and for 3–5 d postsurgery, as well as buprenorphine (0.5 mg/kg s.c.) immediately after injury and for 2 d thereafter. Antibiotics were administered daily until sacrifice, rotating the use of baytril, ciprofloxacin, and ampicillin every 2 wk (2.5 mg/kg dose for all drugs; s.c. delivery for baytril and dissolved in drinking water for ciprofloxacin and ampicillin).

Perfusions and tissue collection

Mice were anesthetized at 6 or 12 wk postinjury and transcardially perfused with PBS, followed by 4% paraformaldehyde. Spinal cord regions corresponding to dorsal roots at T2–T5, T6–T12, and T13-L2 were postfixed overnight in 4% paraformaldehyde, flash frozen at −65°C in isopentane, and stored at −80°C. Number of animals per group and exclusions are detailed in Table IV.

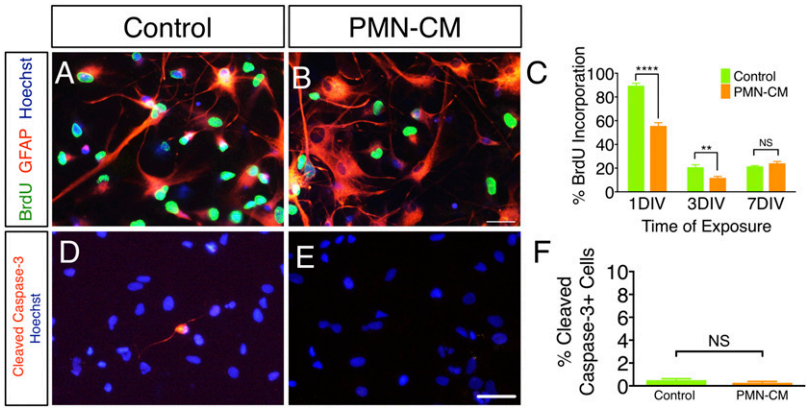

FIGURE 2. PMN-CM decreases hNSC proliferation but does not alter hNSC death under differentiating conditions. (**A** and **B**) BrdU (green fluorescence) incorporation by hNSC treated with DM control or PMN-CM for 1 DIV. Note the increase in $GFAP^+$ (red fluorescence) cell number and altered morphology between DM and PMN-CM. (**C**) PMN-CM treatment (orange bars) decreased the proportion of hNSC with BrdU incorporation versus DM control (green bars) at 1 DIV and 3 DIV, but not 7 DIV (two-way ANOVA, $p < 0.0001$; Bonferroni post hoc, $^{**}p < 0.01$, $^{****}p < 0.0001$). (**D** and **E**) CC3 immunolabeling (red fluorescence) in hNSC exposed to DM control or PMN-CM for 1 DIV. Hoechst (blue fluorescence) indicates total nuclei. (**F**) PMN-CM treatment (orange bar) did not alter $CC3^+$ cells proportion versus DM control (green bars). $n = 2$ technical replicates and $n = 3$–4 biological replicates/condition. Mean ± SEM. Scale bar, 50 μm. Student t test, $p > 0.05$ (NS).

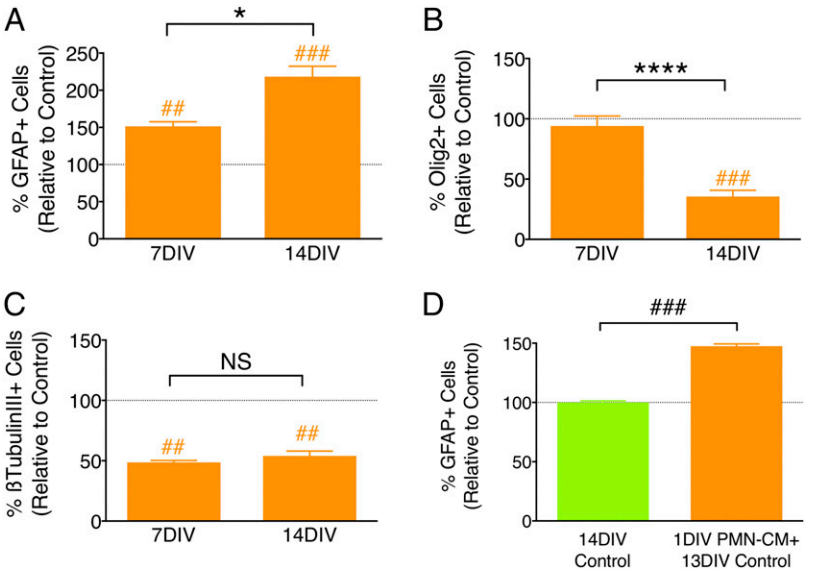

FIGURE 3. PMN-driven astroglial differentiation increases over time and does not require continuous exposure to CM. (**A**–**C**) PMN-CM (orange bars) versus DM control (dashed line) comparisons were conducted using one-sample *t* tests ($^{\#\#}p < 0.01$, $^{\#\#\#}p < 0.001$). Comparisons between groups were performed using one-tailed Student *t* tests ($^{*}p < 0.05$, $^{****}p < 0.0001$). (A) PMN-CM increased the percentage of GFAP$^+$ cells versus DM control by 7 DIV, which was further enhanced by 14 DIV. (B) PMN-CM decreased the percentage of nuclear Olig2$^+$ cells after 14 DIV, but not 7 DIV. (C) PMN-CM decreased the percentage of β-tubulin III$^+$ cells by 7 DIV, which was maintained through 14 DIV. (**D**) Transient 24-h (1 DIV) exposure of hNSC to PMN-CM increased the percentage of GFAP$^+$ cells versus DM control (green bar and dashed line) by 14 DIV. $n = 2$ technical replicates and $n = 3$–4 biological replicates/condition. Mean ± SEM.

Spinal cord immunohistochemistry

The T6–T12 spinal cord region was frozen in isopentane at −55°C and embedded in optimal cutting temperature compound (OCT; Tissue-Tek). Thirty-micrometer–thick parasagittal sections were cut on a freezing microtome, or 30-μm–thick transverse sections were cut using a CryoJane tape transfer system (Leica), as previously described (35, 36). Number of animals cut for each plane is detailed in Table IV. Free-floating sections cut on the microtome were collected in 96-well plates filled with Tris and 0.02% sodium azide and stored at 4°C until processed for immunostaining. CryoJane-cut sections were collected on slides and stored at −20°C until processed for immunostaining. All sectioning and immunostaining procedures were conducted, as previously described (35, 36). Abs and dilutions used are listed in Table II.

Stereological quantification

Cell counts. The Optical Fractionator probe (37) was used for unbiased estimation of the number of hNSC (SC121$^+$), human astrocytes (SC123$^+$), human Olig-2$^+$ cells (SC121$^+$/Olig2$^+$), and human CC1$^+$ cells (SC121$^+$/CC1$^+$) in StereoInvestigator (Microbrightfield). For the number of SC121$^+$ cells, counting areas were determined by drawing contours at every 1-mm region in parasagittal sections using a ×4 objective and at a frequency of one every sixth section. For fate analysis, the counting areas were determined by drawing contours around the entire transverse spinal cord using a ×4 objective and at the frequency of one every 12th section. Cells associated with a visible nucleus indicated by either methyl green (SC121) or hematoxylin (all other fate markers) were counted using a ×100 objective in the corresponding areas. Grid size measurements were determined based on preliminary experimentation to establish a low coefficient of error (CE) (Table V) and sufficient total estimated counts per frame (3–5 cells per counting frame). hNSC migration was reported as the total number of cells within a 1-mm region.

Lesion volume analysis. Lesion volume analysis was performed using fibronectin immunostaining to identify the SCI epicenter in transverse sections and using the Cavalieri estimator probe in StereoInvestigator. The fibronectin-positive region was identified as the lesion epicenter, and a point grid of known spacing (100 μm apart) was randomly overlayed on the section image. Points were counted using a ×20 objective within the region of interest.

Statistical analysis

All analyses were performed by observers blinded to experimental groups. Statistics were performed using Prism 5, version 5.0 (GraphPad Software). All data are presented as mean ± SEM. When percentages are reported, experimental values were normalized to the control condition (DM control). Data were analyzed using one-sample *t* tests to compare with control and Student *t* tests to compare between experimental conditions. When comparing across multiple groups, one-way ANOVA was conducted first, followed by Tukey post hoc tests. In Fig. 2, to compare across multiple time points and multiple groups, two-way ANOVA was conducted, followed by a Bonferroni post hoc *t* test. In all statistical analyses, significance was defined as $p < 0.05$.

Results

CM collected from PMN, but not Mϕ, promotes astroglial differentiation of hNSC

We sought to investigate whether factors generated by innate immune cells could alter hNSC fate and migration in vitro. Details related to both in vitro and in vivo experiments are outlined in Tables I–V. hNSC were cultured with either DM control or CM collected from PMN or Mϕ. We first confirmed that the culture conditions used for CM generation did not lead to significant or differential cell death in PMN or Mϕ. The number of PI$^+$ PMN and Mϕ was quantified using flow cytometry after 24 h of incubation in DM control (Fig. 1A, *Materials and Methods*). An average of 6.04% PMN and 5.27% Mϕ were PI$^+$ (Fig. 1B; no significant differences), suggesting a negligible contribution of death/debris to CM collected. hNSC fate was analyzed by quantification of the number of cells immunolabeled for GFAP (astroglial lineage), nuclear Olig2 (oligodendroglial lineage), and β-tubulin III (neuronal lineage). To confirm the relationship of GFAP expression with astroglial lineage commitment as opposed to maintenance of neural progenitors, we evaluated GFAP in combination with the stem cell markers Nestin and Sox2. Quantitative RT-PCR revealed that GFAP mRNA expression increased with time under differentiation conditions, whereas Nestin mRNA expression did not (*Materials and Methods* and data under Fig. 1C, 1D). In parallel, coimmunolabeling of hNSC for GFAP and Sox2 demonstrated that the number of GFAP$^+$/Sox2$^+$ human neural progenitors under differentiation conditions was <0.284% at 14 DIV (Table VI), suggesting that, by this time point, human cells expressing GFAP are committed to the astroglial lineage.

At 14 DIV, PMN-CM, but not Mϕ-CM, significantly increased the percentage of GFAP$^+$ cells in comparison with DM control (Fig. 1E). Morphologically, PMN-CM exposure resulted in intensely stained GFAP$^+$ cells with extended processes consistent with hypertrophic, reactive astrocytes. In contrast, both PMN-CM and Mϕ-CM decreased the percentage of Olig2$^+$ cells compared with DM control (Fig. 1F), whereas PMN-CM decreased and Mϕ-CM increased the percentage of β-tubulin III$^+$ cells over DM control (Fig. 1G). As described under *Materials and Methods*, all in vitro experiments (Figs. 1–8) were conducted with PMN-CM generated from NOD-*scid* mice to enable comparison with in vivo xenotransplantation data in NOD-*scid* mice (Figs. 9, 10). To

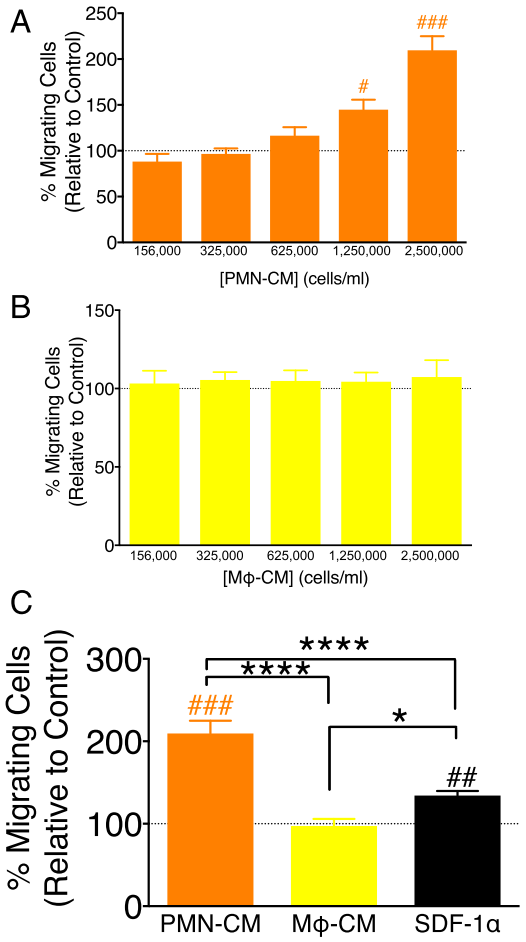

FIGURE 4. PMN-CM promotes hNSC migration in vitro. (**A**–**C**) hNSC migration toward DM control (dashed line), PMN-CM (orange bars), Mϕ-CM (yellow bars), and SDF1α (black bar, positive migration control) was quantified in Transwell assays. CM versus DM control comparisons were conducted using one-sample *t* tests ($^{\#}p < 0.05$, $^{\#\#}p < 0.01$, $^{\#\#\#}p < 0.001$). Comparisons between PMN-CM, Mϕ-CM, and SDF1α groups were conducted using one-way ANOVA, followed by Tukey post hoc tests ($^{****}p < 0.0001$, $^{*}p < 0.05$). (A) Increasing PMN-CM seeding density increased hNSC migration. (B) Increased Mϕ-CM seeding density did not alter hNSC migration. (C) PMN-CM (seeding density 2,500,000 cells/ml) increased hNSC migration versus DM control, Mϕ-CM (seeding density 2,500,000 cells/ml), and SDF1α (200 ng/ml). SDF1α increased hNSC migration versus DM control and Mϕ-CM. $n = 2$ technical replicates and $n = 3$–4 biological replicates/condition. Mean ± SEM.

confirm that the effect of CM on hNSC fate generalized across species as well as to fully immune-sufficient animals, we generated CM generated from Sprague–Dawley rats and verified a parallel astroglial fate shift (Fig. 1H). Taken together, these data suggest that PMN-CM selectively modulates NSC fate.

PMN-mediated increase in GFAP$^+$ cell proportion in differentiating hNSC could be attributed to either increased astroglial lineage selection or increased death of neuronal or oligodendroglial cells. Given that cell cycle exit and differentiation are linked (38), cell proliferation and death were assessed using BrdU incorporation and CC3 staining, respectively. PMN-CM exposure under differentiating conditions transiently decreased the percentage of hNSC exhibiting BrdU incorporation at 1 DIV and 3 DIV, but not at 7 DIV when compared with DM control (Fig. 2A–C). Early decreases in BrdU incorporation were not associated with increased CC3$^+$ cell proportion (Fig. 2D–F), consistent with the induction of differentiation and not cell death. These data suggest that PMN-CM selectively accelerates hNSC differentiation and promotes astroglial lineage selection.

If PMN-CM promotes astroglial lineage selection, we would predict the kinetics of differentiation to demonstrate a steady increase in the proportion of GFAP$^+$ human cells over time, with a corresponding decrease in the proportion of nuclear Olig2$^+$ and/or β-tubulin III$^+$ cells. We quantified the number of GFAP$^+$, nuclear Olig2$^+$, and β-tubulin III$^+$ cells following hNSC exposure to PMN-CM or DM control at 7 versus 14 DIV, as described above. Consistent with a lineage selection mechanism, the percentage of GFAP$^+$ cells increased (Fig. 3A), the percentage of oligodendroglial cells decreased (Fig. 3B), and percentage of neuronal cells remained the same over time (Fig. 3C). A parallel question is whether continuous exposure to PMN-CM throughout the period of differentiation is required, or whether a transient priming or conditioning exposure is sufficient. This is important for in vivo relevance, as PMN infiltration is often transient, including after CNS injury. To test this, hNSC were exposed to PMN-CM or DM control for 24 h, washed, and followed by a 13 DIV incubation in DM. Transient PMN-CM exposure also resulted in an increase in the percentage of GFAP$^+$ cells compared with DM control (Fig. 3D). Taken together, these data suggest that PMN-CM selectively directs NSC differentiation toward an astroglial lineage, and that a transient or priming exposure to factors present in PMN-CM is sufficient to drive lineage commitment.

CM collected from PMN, but not Mϕ, promotes hNSC migration

Innate immune cells synthesize a variety of chemotactic factors that can affect NSC/NPC migration, for example, TNF-α and IFN-γ (39). Microglial-directed NSC migration has been previously demonstrated (15), but the effect of PMN and Mϕ on NSC chemotaxis, and the role of specific factors in these effects, has not been tested. We investigated the effect of PMN-CM and Mϕ-CM on hNSC migration using Transwell (Boyden chamber) chemotactic assays. Transwell assays permit directional assessment of migration if conducted over a short timescale (hours) before concentration differences for the molecule(s) of interest equalize between the upper and lower compartments. However, Transwell assays do not permit evaluation of migration over a linear chemotactic gradient; accordingly, evaluation across an increasing concentration series is used to demonstrate that any observed effects are not the result of random motion (chemokinesis) (40). Using a set incubation period of 3.5 h, we therefore tested this relationship using CM generated from different initial seeding densities (156,000 to 2,500,000 cells/ml) of PMN and Mϕ, and harvesting CM, as described under *Materials and Methods*.

PMN-CM induced a seeding density-dependent increase in hNSC migration (Fig. 4A), suggesting the synthesis of chemotactic factors by PMN. In contrast, Mϕ-CM did not affect hNSC migration even in CM generated from the highest seeding density (Fig. 4B). Direct comparison of 2,500,000 PMN-CM and Mϕ-CM demonstrated a significant increase in hNSC migration in response to PMN-CM and the chemoattractant SDF1α (CXCL12; 200 ng/ml) (41), but not Mϕ-CM (Fig. 4C). SDF1α is a migration signal for many cell types during both development and adulthood (42); neural progenitor cells have been shown to express the SDF1α receptor, CXCR4, as well as to exhibit migration in vitro and in vivo in response to SDF1α (43, 44). Accordingly, SDF1α was employed as a positive migration control. Previous studies have shown that hNSC chemotaxis approaches an active threshold at

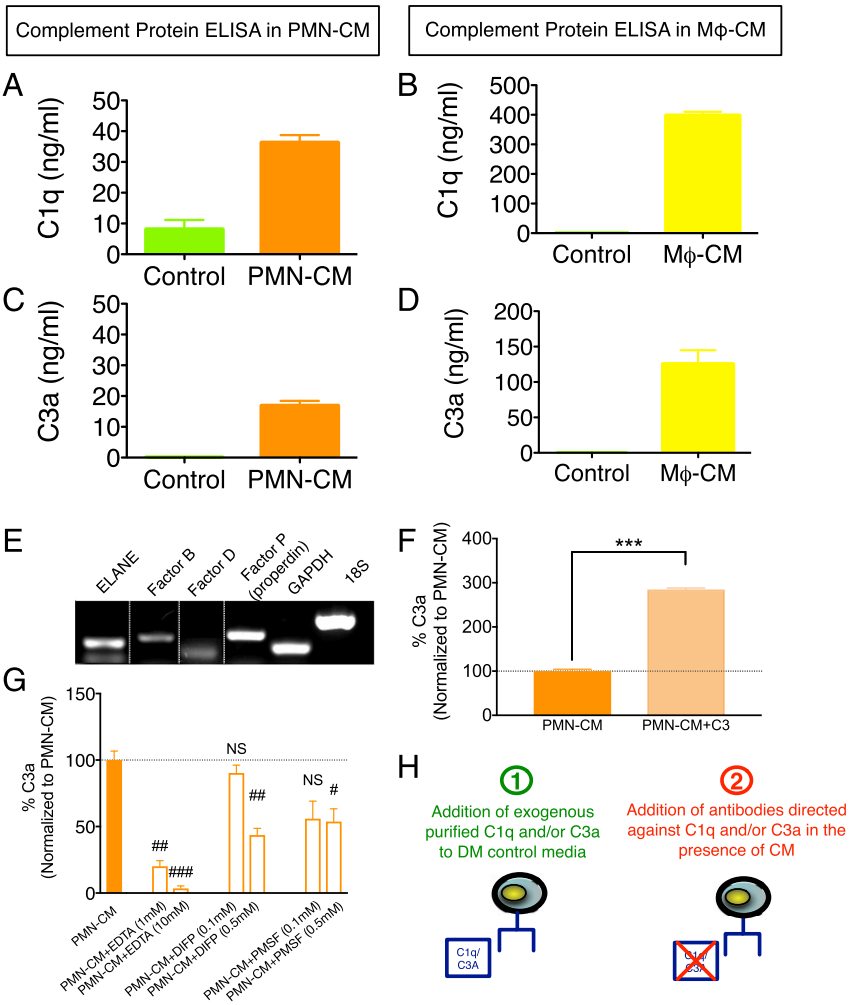

FIGURE 5. PMN synthesize C1q and C3a. (**A–D**) $n = 2$ technical replicates and $n = 3$–4 biological replicates/condition. (A and B) ELISA quantification of C1q in DM control (green bars) versus PMN-CM (orange bars) and Mϕ-CM (yellow bars) revealed 28 and 400 ng/ml, respectively. (C and D) ELISA quantification of C3a in DM control (green bars) versus PMN-CM (orange bars) and Mϕ-CM (yellow bars) revealed 18 and 120 ng/ml, respectively. (**E**) RT-PCR analyses demonstrated constitutive expression of ELANE, factor B, factor D, and properdin (factor P) by PMN. The dotted lines indicate where parts of the image were joined. (**F** and **G**) $n = 2$ technical replicates and $n = 3$ biological replicates/condition. (F) ELISA measurement of C3a generation by cultured PMN (orange bar) and cultured PMN to which 1 μg/ml C3 was added (light orange bar). C3 addition to PMN resulted in a significant increase in C3a present in PMN-CM (Student t test, $^{***}p < 0.001$). (G) ELISA measurement of C3a generation by PMN in the presence of EDTA, DIFP, or PMSF at the indicated concentrations. PMN-CM shown as orange bar and dashed line. Both divalent cation chelation and serine protease inhibition resulted in significant decreases in C3a present in PMN-CM (one-sample t test versus PMN-CM; $^{\#}p < 0.05$, $^{\#\#}p < 0.01$, $^{\#\#\#}p < 0.001$). (**H**) Diagram illustrating the two approaches used to test the role of C1q and/or C3a in mediating cell fate and migration in Figs. 6–8: 1) addition of exogenous purified C1q and/or C3a to DM control media (in the absence of PMN-CM and/or Mϕ-CM), and 2) addition of Abs directed against C1q and/or C3a in the presence of PMN-CM. Mean ± SEM.

100 ng/ml and the chemotactic index remains stable for SDF1α concentrations between 100 and 1000 ng/ml (41). In the current study, the chemotactic response of hNSC to PMN-CM was 1.5 times greater than SDF1α at 200 ng/ml (209.5 versus 134.2%, respectively), suggesting that the soluble factors present in PMN-CM exert a robust and strong effect on hNSC migration. Furthermore, the absence of an enhanced chemotactic response to Mϕ-CM suggests either that soluble factors specific to PMN-CM induce migration, or that hNSC migration is modulated in a dose-dependent manner by factors present at different concentrations in PMN-CM versus Mϕ-CM.

PMN- and Mϕ-CM factors

PMN and Mϕ synthesize multiple cytokines and chemokines, including TNF-α (24, 45, 46). As well, we and others have shown that some components of the complement cascade, specifically C1q and C3, are synthesized by PMN and Mϕ both in vitro and in vivo following neurodegeneration (47–49). Both C1q and C3a, a cleavage product of C3, have been reported to direct cell migration (49–51). Additionally, C3a has been reported to modulate neurogenesis and neuronal fate in mouse neural progenitors (52). We hypothesized that one or more of these components could modulate NSC fate and migration.

To test this hypothesis, we first established the concentrations of C1q and C3a in CM via ELISAs (Fig. 5A–D). Mϕ-CM contained significantly higher concentrations of both C1q and C3a (Fig 5B, 5D; 400 and 120 ng/ml, respectively) compared with PMN-CM (Fig 5A, 5C; 28 and 18.5 ng/ml, respectively). To identify whether interaction between PMN/Mϕ-generated C1q/C3a and hNSC was possible, we verified the expression of the gC1qR and C3aR by hNSC via PCR (Supplemental Fig. 1A). In parallel, we tested whether treatment of hNSC with CM induces signaling pathway activation that is dependent upon the presence of complement proteins. Phosphoarray analysis of intracellular signaling pathways identified p-AKT and p-ERK as strongly activated after treatment of hNSC with C1q and C3a. Quantification of p-AKT and p-ERK in immunoblots from hNSC treated with PMN-CM generated from wild-type, C1qKO, or C3KO mice showed that activation of p-AKT signaling was blocked in both C1qKO and C3KO PMN-CM, whereas activation of p-ERK signaling was blocked in C3KO but not C1qKO PMN-CM (Supplemental Fig. 1B–D). Altogether, these data suggest that C1q and C3a play a role in PMN-CM–induced signaling pathway activation in hNSC.

Critically, C3 must be cleaved to generate active C3a. Proteolytic cleavage of C3 to C3a and other C3 fragments can occur via the classical and alternative complement pathways and their C3 convertases, which are Ca^{2+}/Mg^{2+} dependent. PMN synthesize and secrete factor B as well as factor D (Fig. 5E), which are required for C3(H20)Bb and fC3bFb alternative pathway convertase formation (50, 51, 53, 54). This process can be triggered spontaneously, via generation of C3(H20) in the fluid phase. Critically, although C3bBb is more active than C3(H20)Bb, generating 2-fold the amount of C3a, factor B has a greater affinity for C3(H20), and the resistance of

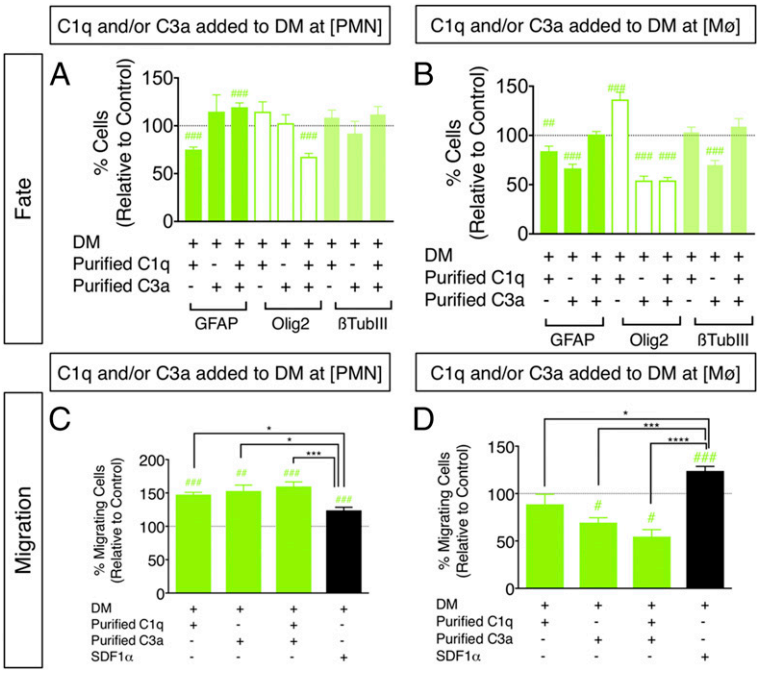

FIGURE 6. Treatment of hNSC with purified C1q and C3a modulates hNSC fate and migration in vitro. (**A** and **B**) hNSC were treated with purified C1q and/or C3a at [PMN] or [Mϕ], followed by immunocytochemical quantification of $GFAP^+$, nuclear $Olig2^+$, and β-tubulin III^+ cell number. Comparisons versus DM control (dashed line) were conducted using one-sample *t* tests ($^{\#}p < 0.05$, $^{\#\#}p < 0.01$, $^{\#\#\#}p < 0.001$). hNSC differentiation in the presence of C1q plus C3a[PMN], but not C1q plus C3a[Mϕ] increased the percentage of $GFAP^+$ cells and decreased the percentage of $Olig2^+$ cells at 14 DIV compared with DM control. (**C** and **D**) hNSC were treated with purified C1q and/or C3a at [PMN] or [Mϕ], followed by Transwell assay quantification of migration, respectively. Comparisons versus DM control (dashed line) were conducted using one-sample *t* tests ($^{\#}p < 0.05$, $^{\#\#}p < 0.01$, $^{\#\#\#}p < 0.001$). Comparisons across multiple groups were conducted using one-way ANOVA [(C): $F = 8.513$, $p < 0.0005$; (D): $F = 18.84$, $p < 0.0001$], followed by Tukey post hoc tests ($^{*}p < 0.05$, $^{***}p < 0.001$, $^{****}p < 0.0001$). Addition of C1q[PMN], C3a[PMN], and C1q plus C3a[PMN] increased hNSC migration versus DM control, and relative to SDF1α. Addition of C3a[Mϕ] and C1q plus C3a[Mϕ] decreased hNSC migration versus DM control, and relative to SDF1α. $n = 2$ technical replicates and $n = 3$–4 biological replicates/condition. Mean ± SEM.

C3(H20)Bb to inactivation results in prolonged activity (55). PMN also synthesize and secrete properdin (Fig. 5E), which, in combination with C3b membrane binding, amplifies convertase activity and C3a generation (54, 56, 57). Additionally, C3 can undergo direct cleavage by neutral and serine proteases, generating C3a (58, 59). Finally, PMN secrete elastases (e.g., ELANE, Fig. 5E), and ELANE efficiently cleaves C3 into biologically active C3a (59). To test for fluid-phase C3a generation, purified C3 was added to cultured PMN in vitro and C3a measured by ELISA in PMN-CM. C3 addition to PMN increased C3a in PMN-CM (Fig. 5F). Conversely, addition of either the divalent cation chelator EDTA or protease inhibitors (DIFP or PMSF) to cultured PMN decreased C3a in PMN-CM in a dose-dependent manner (Fig. 5G). These data are consistent with early demonstrations of PMN-derived cationic and neutral protease C3 cleavage and C3a generation (60, 61), as well as recent studies of ELANE C3 cleavage and C3a generation (59). Critically, in this regard, inhibition of C3a generation by EDTA in our data does not necessarily reflect C3 convertase inhibition, as EDTA has been shown to bind and inhibit ELANE (62). Collectively, these data suggest that PMN-CM not only contains C3a, but can process C3 to generate C3a.

Based on these data, we investigated the role of C1q and C3a in the modulation of hNSC fate and migration using two approaches (Fig. 5H): 1) addition of exogenous purified C1q and/or C3a alone or in combination to DM control conditions, that is, in the absence of PMN-CM or Mϕ-CM, and 2) addition of Abs directed against C1q and/or C3a alone or in combination to PMN-CM or DM control conditions.

Addition of purified C1q and/or C3a modulates p-AKT/p-ERK signaling, hNSC fate, and hNSC migration

For the first approach, hNSC were cultured with either DM control or DM with the addition of purified C1q and/or C3a at the concentrations measured in CM, referred to as C1q plus C3a[PMN] and C1q plus C3a[Mϕ]. The effect of purified C1q plus C3a[PMN] and C1q plus C3a[Mϕ] on p-AKT and p-ERK signaling was verified, as described above, supporting the activity of these molecules independent of other CM components (Supplemental Fig. 1E, 1F). hNSC fate was analyzed by quantification of the number of cells immunolabeled for GFAP, nuclear Olig2, and β-tubulin III after 14 DIV, as shown above in Fig. 1E–G. Both C1q and C3a exhibited independent effects on hNSC differentiation. For example, C1q[PMN] decreased the percentage of $GFAP^+$ cells only (Fig. 6A), whereas treatment with C1q [Mϕ] decreased the percentage of $GFAP^+$ cells, increased $Olig2^+$ cells, and did not alter β-tubulin III expression at 14 DIV (Fig. 6B). With respect to C3a, C3a[PMN] did not alter the percentage of $GFAP^+$, $Olig2^+$, or β-tubulin III^+ cells identified (Fig. 6A). Conversely, treatment with C3a[Mϕ] decreased the percentage of cells exhibiting GFAP, Olig2, and β-tubulin III expression at 14 DIV (Fig. 6B). These effects were not related to cell death, as there were no increases in the number of $CC3^+$ cells across treatment conditions (Table VII). Critically, however, combined addition of C1q plus C3a is most relevant for comparison with CM treatment in which both C1q and C3a are present. C1q plus C3a[PMN] increased the percentage of $GFAP^+$ cells, whereas C1q plus C3a[Mϕ] did not (Fig. 6A, 6B, Supplemental Fig. 2A). Additionally, both C1q plus C3a[PMN] and C1q plus C3a[Mϕ] resulted in a significant decrease in the percentage of $Olig2^+$ hNSC compared with control (Fig. 6A, 6B, Supplemental Fig. 2B). These effects are consistent with those observed when hNSC were differentiated in PMN- and Mϕ-CM (Fig. 1). However, neither C1q plus C3a[PMN] nor C1q plus C3a[Mϕ] altered the percentage of β-tubulin III^+ hNSC (Fig. 6A, 6B, Supplemental Fig. 2C), suggesting that factors other than C1q and C3a mediate the effect of CM on this aspect of hNSC fate. Critically, addition of purified C3a-desArg to hNSC did not alter cell fate with respect to GFAP, Olig2, or β-tubulin III^+ cells (Supplemental Fig. 2D), and mRNA for C5L2, one of the known receptors for C3a-desArg, was not detected in hNSC samples (Supplemental Fig. 2E). These data demonstrate that the effects of C3a in this in vitro study cannot be attributed to C3a-desArg. Collectively, it can be concluded that C1q and C3a exert specific, concentration-dependent effects on hNSC and may operate interactively to modulate hNSC differentiation.

In parallel with hNSC fate, the effect of purified C1q and/or C3a on hNSC migration was tested using Transwell chemotactic assays, as described above, for PMN-CM and Mϕ-CM. SDF1α (200 ng/ml) was included as a positive control in all migration experiments, as above (black bars, Fig. 6C, 6D). hNSC exhibited increased migration toward C1q[PMN], C3a[PMN], and C1q plus

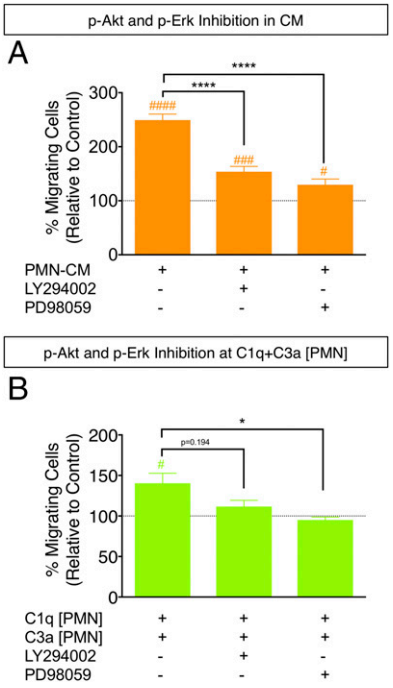

FIGURE 7. Inhibition of AKT/ERK signaling blocks hNSC migration in PMN-CM and in response to C1q plus C3a[PMN]. Comparisons versus DM control (dashed line) were conducted using one-sample *t* tests ($^{\#}p < 0.05$, $^{\#\#\#}p < 0.001$, $^{\#\#\#\#}p < 0.0001$). Comparisons across multiple groups were conducted using one-way ANOVA, followed by Tukey post hoc tests ($^{*}p < 0.05$, $^{****}p < 0.0001$). PI3K/AKT signaling was inhibited by LY294002 (50 μM, 3.5 h). ERK signaling was inhibited by PD98059 (10 μM, 3.5 h). (**A**) Comparison of treatment with PMN-CM versus PMN-CM in the presence of PI3K/AKT or ERK pathway inhibitors revealed significant attenuation of hNSC migration (one-way ANOVA; $F = 36.72$, $p < 0.0001$), although some chemotactic activity was retained. (**B**) Comparison of treatment with C1q plus C3a[PMN] versus C1q plus C3a[PMN] in the presence of PI3K/AKT or ERK pathway inhibitors showed that PD98059 blocked, and LY294002 exhibited a trend for attenuation of, hNSC migration (one-way ANOVA; $F = 4.355$, $p < 0.05$). Although C1q plus C3a [PMN] versus C1q plus C3a[PMN] plus LY294002 did not reach significance in post hoc testing, the presence of both LY294002 and PD98059 prevented hNSC migration versus control. $n = 3$ technical replicates and $n = 3$ biological replicates/condition. Mean ± SEM.

C3a[PMN] compared with both DM control and SDF1α (Fig. 6C). In contrast, addition of C1q plus C3a[Mϕ] significantly decreased hNSC migration compared with DM control and SDF1α (Fig. 6D), suggesting a repulsive effect. Interestingly, concentration-dependent chemoattraction versus chemorepulsion (fugetaxis) is consistent with previous reports for PMN and T cell responses to IL-8 and SDF1α gradients in vitro and in vivo (63, 64). In particular, higher concentrations of IL-8 and greater CXCR2 occupancy in human PMN were associated with conversion from chemoattraction to chemorepulsion (63); moreover, both chemoattraction and chemorepulsion were sensitive to PI3K/AKT inhibitors. These findings parallel our observations of PI3K/AKT activation by C1q plus C3a [PMN] and C1q plus C3a[Mϕ], and are consistent with reports by Tharp et al. (63) that chemorepulsion control lies downstream of PI3K/AKT.

As a test of the biological activity of signaling induced by purified C1q and C3a on hNSC, we assayed the effects of PMN-CM and C1q plus C3a[PMN] on hNSC in the presence and absence of PI3K/AKT and ERK pathway inhibitors (LY294002 and PD98059, respectively), and used hNSC migration as a functional readout in which cellular toxicity is minimized due to the short-term incubation. hNSC migration induced by PMN-CM (Fig. 7A) was significantly attenuated by both PI3K/AKT and ERK pathway inhibition (one-way ANOVA, $p < 0.0001$, $F = 36.72$, followed by post hoc Tukey test: $p < 0.0001$ for PMN-CM versus LY294002, $p < 0.0001$ for PMN-CM versus PD98059), although a small but significant increase over control remained (one-sample *t* test: $p < 0.001$ for LY294002 versus control, $p < 0.05$ for PD98059 versus control). In parallel, hNSC migration induced by C1q plus C3a[PMN] (Fig. 7B) was completely blocked by ERK pathway inhibition (one-way ANOVA, $p = 0.0222$, $F = 4.355$, followed by Tukey post hoc test: $p < 0.05$ for C1q plus C3a[PMN] versus PD98059), and a strong trend for blockade was observed with PI3K/AKT pathway inhibition (one-way ANOVA, $p < 0.05$, $F = 4.355$, followed by Tukey post hoc test: $p > 0.05$ for C1q plus C3a[PMN] versus PD98059). In addition, C1q plus C3a[PMN] failed to induce migration versus control in the presence of PI3K/AKT or ERK inhibition (one-sample *t* test: $p > 0.05$ for LY294002 versus control, $p > 0.05$ for PD98059 versus control). Taken together, these data support concentration gradient-dependent effects of complement proteins on hNSC migration and indicate that these effects are mediated by activation of intracellular signaling pathways, suggesting a receptor-mediated mechanism.

Blockade of C1q and C3a in PMN-CM reduces astroglial differentiation and migration

In the second approach, hNSC were cultured in either PMN-CM or PMN-CM with the addition of Abs directed against C1q (αC1q Ab) and/or C3a (αC3a Ab). As described under *Materials and Methods*, blocking Abs were selected based on previously published studies. hNSC fate analysis was restricted to quantification of the number of cells immunolabeled for GFAP. Addition of αC1q Ab and/or αC3a Ab to PMN-CM under differentiating conditions significantly decreased the percentage of $GFAP^+$ cells compared with PMN-CM alone (Fig. 8A, Supplemental Fig. 2F, 2G). In contrast, addition of IgG control Abs (Table I) to hNSC cultured in PMN-CM (Supplemental Fig. 2H), or addition of αC1q and/or αC3a to hNSC cultured under DM control conditions (Fig. 8B), had no effect. Similarly, we targeted an alternative PMN-secreted candidate, TNF-α, which has been shown to promote astrocytic differentiation in vitro (39, 65, 66). αTNF-α Ab treatment of either DM or PMN-CM did not alter $GFAP^+$ fate proportion (Fig. 8C). These data support the specificity of the effects on $GFAP^+$ cell fate observed with αC1q Ab and αC3a Ab treatment, and a novel role for C1q and C3a in hNSC fate.

In parallel with hNSC fate, the effect of αC1q Ab and αC3a Ab treatment on hNSC migration in the presence of PMN-CM was tested using Transwell chemotactic assays. SDF1α (200 ng/ml) was included as a positive control in all migration experiments (black bars, Fig. 8D–F). Addition of αC1q Ab and αC3a Ab to PMN-CM, both individually and in combination, significantly decreased migration compared with PMN-CM alone (Fig. 8D). Addition of αC1q Ab and αC3a Ab to DM control media had no effect on hNSC migration (Fig. 8E). IgG control Abs raised in the same species did not alter migration when added to PMN-CM, supporting the specificity of αC1q Ab– and αC3a Ab–directed blockade (Supplemental Fig. 2I). Additionally, although hNSC are responsive to SDF1α, we found that PMN isolated under our conditions do not express SDF1α mRNA (Fig. 8F). We therefore tested addition of an αSDF1α blocking Ab to PMN-CM as a negative control. As predicted, whereas αSDF1 Ab mitigated SDF1α-induced migration (Fig. 8F, gray bar), addition of αSDF1α Ab to either DM control (Fig. 8F, green bar) or PMN-CM (Fig. 8F, orange bars) had no effect on hNSC migration. Altogether, these data support the specificity of αC1q Ab– and αC3a Ab–directed blockade and demonstrate that C1q and C3a are two key PMN-synthesized molecules modulating hNSC fate and migration.

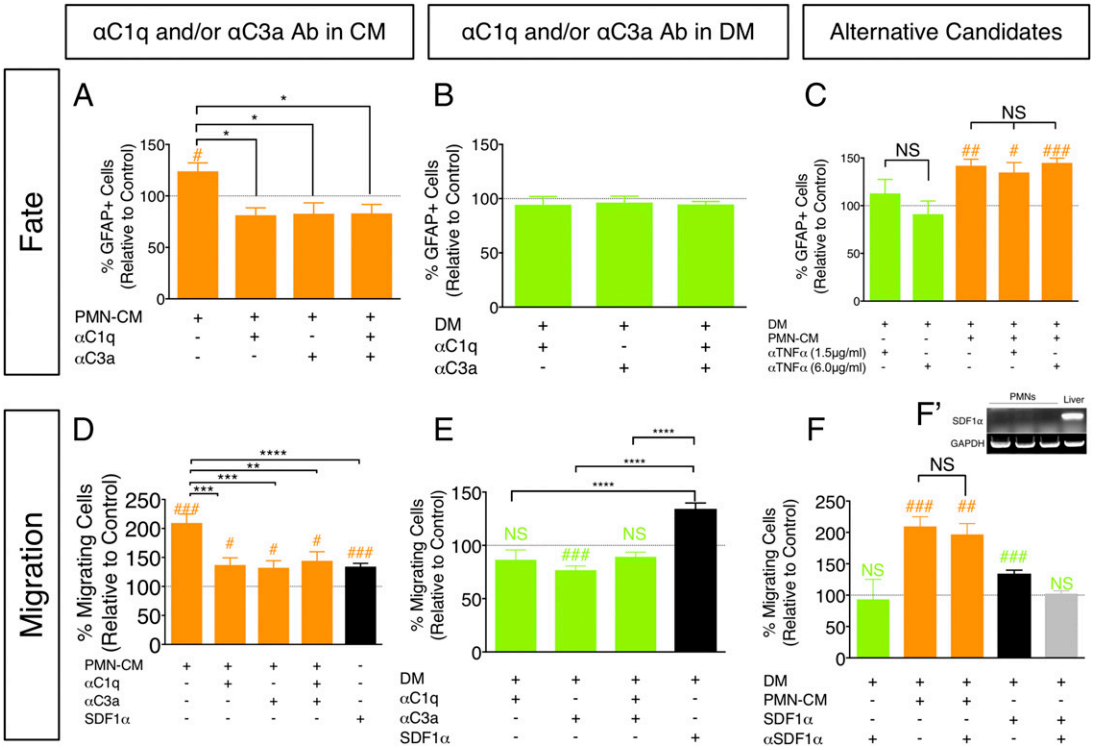

FIGURE 8. Treatment of hNSC with αC1q and αC3a Abs blocks PMN-CM–induced effects on astroglial fate and migration in vitro. (**A**–**F**) hNSC were treated with PMN-CM (orange bars) or DM control (green bars) with or without addition of αC1q and αC3a Abs for 7 DIV. Black bars indicate SDF1α (positive control for Transwell migration). Comparisons versus DM control (dashed line) were conducted using one-sample *t* tests (NS is $p \geq 0.05$, $^{\#}p < 0.05$, $^{\#\#}p < 0.01$, $^{\#\#\#}p < 0.001$). Comparisons between treatment conditions were conducted using one-way ANOVA, followed by Tukey post hoc tests (NS is $p \geq 0.05$, $^{*}p < 0.05$, $^{**}p < 0.01$, $^{***}p < 0.001$, $^{****}p < 0.0001$). (A) hNSC treatment with PMN-CM plus αC1q/αC3a alone or in combination decreased GFAP$^+$ cell number (one-way ANOVA, $F = 6.394$, $p < 0.01$). (B) hNSC treatment with DM control plus αC1q/αC3a alone or in combination did not alter GFAP$^+$ cell number (one-way ANOVA, $F = 0.0335$, $p > 0.05$). (C) hNSC treatment with either DM control (green bars) or PMN-CM plus αTNF-α (orange bars) did not alter GFAP$^+$ cell number (one-way ANOVA, $F = 4.913$, $p < 0.01$). (D) hNSC migration toward PMN-CM was decreased in the presence of αC1q/αC3a Ab alone or in combination (one-way ANOVA, $F = 8.135$, $p < 0.0001$). Treatment with both Abs prevented ~76% hNSC chemotaxis. (E) hNSC migration was unaltered in the presence of αC1q plus αC3a Ab (one-way ANOVA, $F = 22.38$, $p < 0.0001$). (F) hNSC migration was unaltered for DM versus DM plus αSDF1 (green bar), and for PMN-CM versus PMN-CM plus αSDF1 (orange bars; one-way ANOVA, $F = 13.44$, $p < 0.0001$). αSDF1α Ab activity was verified by reversal of SDF1α-induced hNSC migration (black bar, one-sample *t* test SDF1α versus DM control $^{\#\#\#}$; gray bar, one-sample *t* test SDF1α plus αSDF1α versus DM control NS). (**F′**) RT-PCR did not detect mRNA expression of SDF1α by PMN. For (A–F), $n = 2$ technical replicates and $n = 3$–4 biological replicates/condition. Mean ± SEM.

Treatment with αC1q and αC3a Ab in vivo transiently alters hNSC migration and reduces astroglial fate

Based on these in vitro data, we sought an in vivo parallel. We have previously shown that the time of hNSC transplantation into the parenchyma adjacent to the SCI epicenter is a key variable for the in vivo fate and migration profile of engrafted donor human cells. hNSC in this paradigm are multipotent at the time of transplantation and responsive to migration and fate cues in the local microenvironment. Delayed hNSC transplantation (9–30 d post-SCI) results in donor human cell migration away from the SCI epicenter, toward the distal rostral and caudal spinal cord, and predominant oligodendroglial differentiation (33, 34, 67). Conversely, we have recently demonstrated that acute hNSC transplantation (0 d post-SCI) results in increased donor human cell migration toward the SCI epicenter and a pronounced shift toward astroglial fate in the donor human cells that engraft adjacent to it; critically, both of these effects are blocked by Ly6G-mediated depletion of acute PMN infiltration to the injury epicenter (68).

We therefore sought to test the effect of C1q and C3a blockade using αC1q plus αC3a Ab treatment on hNSC migration and fate in this acute SCI transplantation paradigm. We predicted that administration of αC1q plus αC3a Ab at the SCI epicenter would block recruitment of hNSC toward the SCI epicenter, increasing migration toward the rostral and caudal spinal cord, and reduce the astroglial fate shift of donor hNSC. We first verified that C1q and C3 cleavage products are present at the SCI epicenter during the acute period using SDS-PAGE and immunoblotting in 3-mm segments extending rostral and caudal from the lesion (Supplemental Fig. 3). In vivo studies were conducted in NOD-*scid* mice to enable survival of donor human cells, as described previously (33, 34, 67, 68) and under *Materials and Methods*. Importantly, although NOD-*scid* mice exhibit deficits in adaptive immunity, they demonstrate innate immune responses and histopathological characteristics comparable to other mouse strains following SCI (22, 23).

hNSC were transplanted into the intact parenchyma of NOD-*scid* mice adjacent to the SCI epicenter immediately after a moderate contusion injury, as previously described (33, 34, 67, 68). Mice received a single epicenter injection of either vehicle or αC1q plus αC3a Abs at the time of transplantation. We confirmed that administration of αC1q plus αC3a Ab did not alter total hNSC engraftment or SCI lesion volume. Quantification was performed by unbiased stereological analysis of immunohistochemistry for the human specific cytoplasmic marker SC121 with the optical fractionator probe, and of immunohistochemistry for firbronectin as a

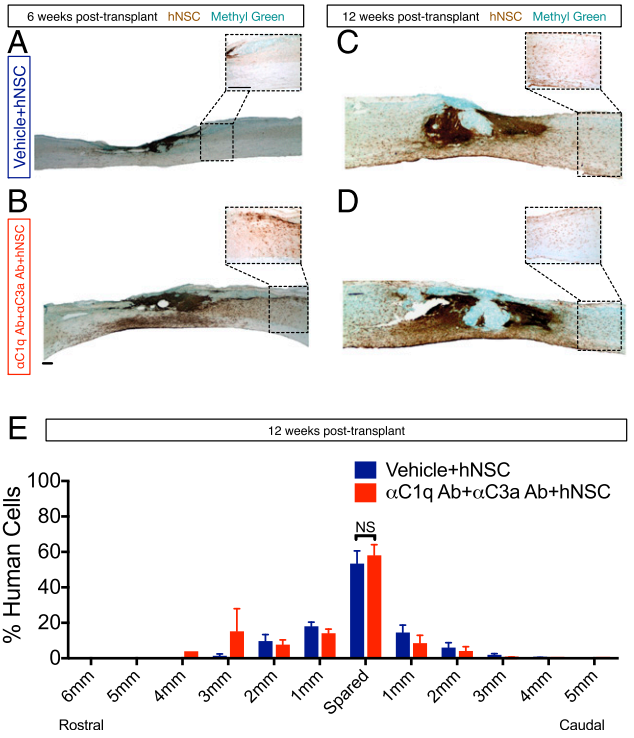

FIGURE 9. αC1q Ab plus αC3a Ab injection transiently promotes migration of donor hNSC away from the injury epicenter in vivo. Six or 12 wk posttransplant, mice were transcardially perfused and tissue collected for histology. (**A**–**D**) Immunohistochemistry in parasagittal spinal cord sections for the human specific cytoplasmic marker SC121 (brown; scale bars, 250 μm); methyl green counterstain at 6 and 12 wk posttransplant. Dashed line insets outline a higher magnification image distal to the injury epicenter. (A and B) At 6 wk posttransplant, a dense plexus of hNSC was present near the injury epicenter in the absence of αC1q and αC3a Abs (A), but many cells migrated away from the lesion in the presence of both Abs (B). (C and D) By 12 wk posttransplant, animals receiving vehicle (C) and those receiving both Abs (D) demonstrated similar migration patterns. (**E**) At 12 wk posttransplant, migration of hNSC was quantified using unbiased stereology and the optical fractionator probe in SCI mice that received vehicle plus hNSC (blue bars) and those receiving αC1q plus αC3a Abs plus hNSC (red bars). The number of $SC121^+$ cells was quantified in the spared tissue around the injury epicenter (spared), as well as in 1-mm regions rostral and caudal to the spared tissue. The number of $SC121^+$ cells found in each region was divided by the total number of SC121 cells quantified for each group (as demonstrated in Supplemental Fig. 4A) to calculate the percentage of human cells in each region. Of particular importance, no significant differences were found in the area marked as the spared tissue between groups. Comparisons were conducted using Student *t* tests (NS is $p > 0.05$). Mean ± SEM is shown.

marker for lesion volume with the Cavalieri probe. There were no differences in either the total number of hNSC (Supplemental Fig. 4A, 4B), or $fibronectin^+$ lesion volume (Supplemental Fig. 4C, 4D) in transplanted mice receiving vehicle versus αC1q plus αC3a Ab. Acute injection of IgG control Abs also did not alter the average lesion volume (Student two-tailed *t* test, $p > 0.05$).

Migration of engrafted hNSC was assessed histologically at 6 wk posttransplantation, and histologically and quantitatively via analysis of hNSC stereological engraftment data for $SC121^+$ cells at 12 wk posttransplant. At 6 wk posttransplant, histological analyses suggested increased hNSC migration away from the epicenter (Fig. 9A, 9B); however, this effect was not sustained at 12 wk (Fig. 9C–E). These data suggest that the effect of complement blockade on hNSC migration was transient, or that a single epicenter injection of these Abs was insufficient.

Fate of engrafted hNSC was assessed quantitatively 12 wk posttransplantation. Quantification was performed by unbiased stereological analysis of immunohistochemistry for the human specific astroglial marker SC123, colabeling for SC121 and the oligoprogenitor marker nuclear Olig2, and colabeling for SC121 and the mature oligodendroglial marker CC1, using the optical fractionator probe. There was a significant decrease in the number of $SC123^+$ cells (hAstrocytes) in αC1q plus αC3a Ab–treated animals (Fig. 10A, 10D). The number of nuclear $Olig2^+$ human oligoprogenitors ($hOlig2^+$ cells) also decreased in αC1q plus αC3a Ab–treated animals (Fig. 10B, 10E); however, the number of $CC1^+$ human oligodendrocytes ($hCC1^+$ cells) did not change (Fig. 10C, 10F), suggesting the absence of a net effect on mature oligodendroglial numbers. In vehicle-treated mice, hAstrocytes, hOlig2, and $hCC1^+$ cells accounted for 100% of engrafted hNSC; in contrast, in αC1q plus αC3a Ab–treated mice, these markers accounted for only 84% of engrafted hNSC (Fig. 10G), suggesting an increase in either other markers or the undifferentiated human donor cell population. Although a caveat with respect to the effect of αC1q plus αC3a Ab administration in vivo is that neutralizing Ab injection could also have altered leukocyte infiltration or other factors, for example, PMN number or density at the SCI epicenter, these data demonstrate a striking effect of a single injection of αC1q plus αC3a Abs on early hNSC migration in combination with a sustained effect on fate. Accordingly, the collective data provide an in vivo parallel for the effect of complement blockade on hNSC fate.

Discussion

This study identifies a novel and important role for cellular and molecular components of the innate immune response in hNSC fate and migration. We demonstrate that PMN-CM induces hNSC astrogliogenesis and promotes hNSC migration, that these effects are replicated by administration of purified C1q and C3a, and that these effects are blocked by Abs directed against these proteins. Furthermore, proof-of-concept data support an in vivo parallel, as a single acute injection of αC1q plus αC3a Ab into the SCI epicenter transiently inhibited hNSC migration toward the lesion and reduced astroglial differentiation of donor human cells in this paradigm.

C1q circulates in plasma predominantly in C1 complex with the proenzymes C1r and C1s (69). However, C1q can be synthesized in the absence of C1r and C1s by a variety of cell types, including PMN (47, 70, 71). Furthermore, a large body of evidence has shown upregulation of C1q in the CNS following injury/disease/aging (72–74), suggesting that C1q alone may have nontraditional functions (75, 76). In contrast, all known functions of C3 are mediated by its cleavage products, C3b and C3a. C3b is involved in opsonization as well as C5 convertase and membrane attack complex (C5b-9) formation, whereas C3a is an anaphylatoxin with potent chemotactic activity through the C3aR. C3a expression has been associated with basal and ischemia-induced hippocampal neurogenesis (52, 77) as well as SDF1α-induced migration and neuronal differentiation of rodent NPC (78). Once formed, C3a is rapidly cleaved by one or more carboxypeptidases (including N, R, and B) to form C3a-desArg (79). Many cells can synthesize and secrete carboxypeptidases, including neurons, which have been shown to produce carboxypeptidase B. However, we demonstrate that the hNSC tested in this work neither express the putative C3a-desArg receptor C5L2, nor exhibit a response to purified C3a-desArg, supporting a primary role for C3a. Critically, however, although we demonstrate that hNSC express gC1qR and C3aR mRNA, C1q and C3a could interact with other receptors. Further investigations to define the interactions of C1q, C3a, and C3a-desArg, as well as the receptors mediating their effects on NSC fate and migration, are in progress. However, our collective

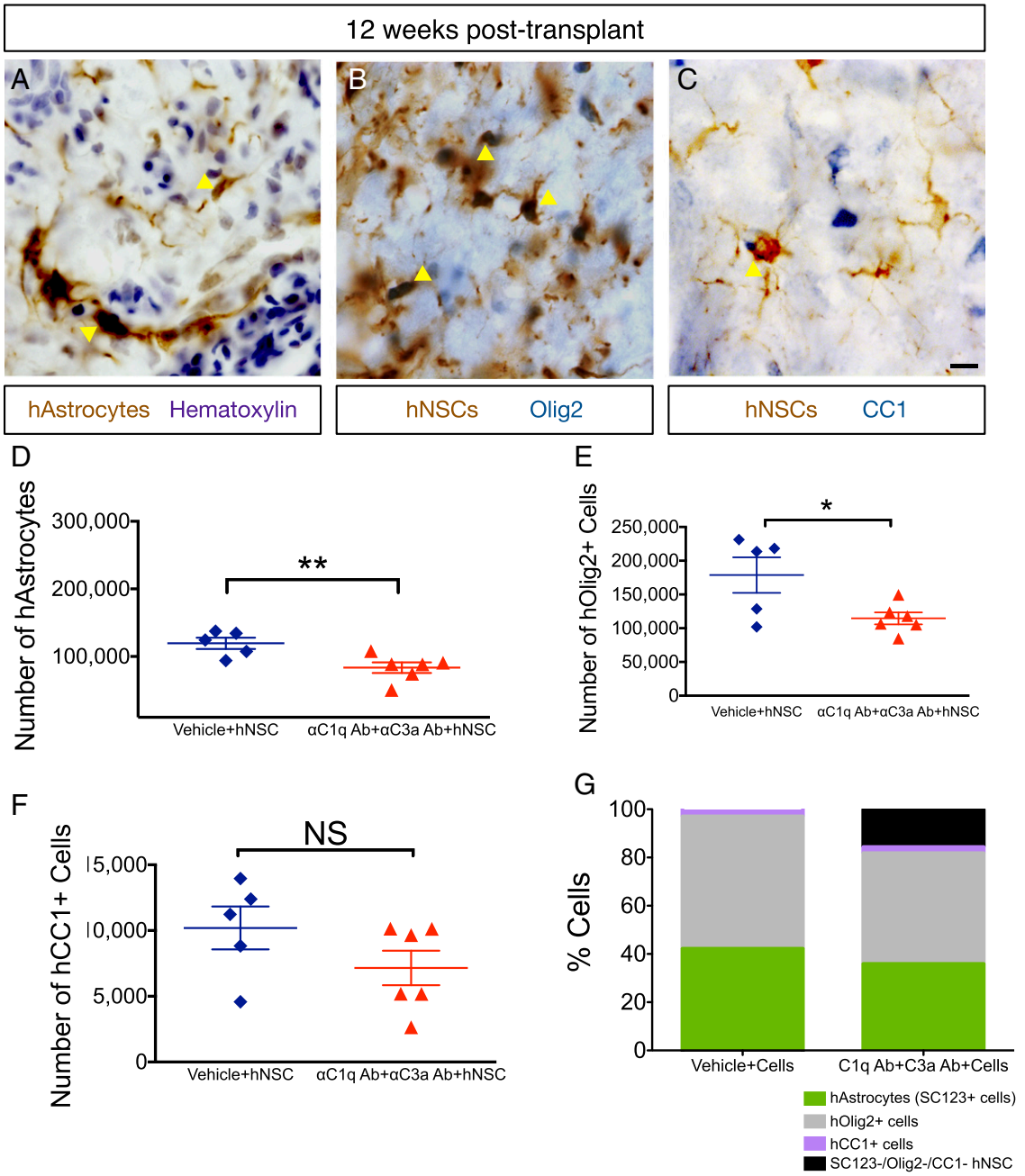

FIGURE 10. αC1q Ab plus αC3a Ab injection reduces glial differentiation in vivo. Twelve week posttransplant, mice were transcardially perfused and tissue collected for histology. (**A**) Immunohistochemistry in transverse spinal cord sections for the human specific astrocytic marker, SC123 (brown); hematoxylin counterstain (purple) at 12 wk posttransplant. Yellow arrowheads indicate human astrocytes (hAstrocytes) that were quantified for unbiased stereology in (**D**). (**B**) Immunohistochemistry in transverse spinal cord sections for the human cytoplasmic marker, SC121 (brown); oligodendroglial progenitors were identified using nuclear Olig2 (blue) at 12 wk posttransplant. Yellow arrowheads indicate human $Olig2^+$ cells (hOlig2) that were quantified for unbiased stereology in (**E**). (**C**) Immunohistochemistry in transverse spinal cord sections for the human cytoplasmic marker, SC121 (brown); mature oligodendroglial marker, CC1 (blue), at 12 wk posttransplant. Yellow arrowheads indicate human $CC1^+$ cells (hCC1) that were quantified for unbiased stereology in (**F**). (D–F) At 12 wk posttransplant, fate of hNSC was quantified using unbiased stereology and the optical fractionator probe in SCI mice that received vehicle plus hNSC (blue diamonds) and those receiving αC1q plus αC3a Abs plus hNSC (red triangles). Comparisons were conducted using Student *t* tests (NS is $p > 0.05$, $*p < 0.05$, $**p < 0.01$). (D and E) In the presence of αC1q plus αC3a Abs, the number of hAstrocytes (D) and $hOlig2^+$ cells (E) significantly decreased compared with control (vehicle plus hNSC), but the number of $hCC1^+$ cells remained unaltered as a result of Ab injection (F). (**G**) In mice receiving vehicle plus hNSC, hAstrocytes, $hOlig2^+$, and $hCC1^+$ cells accounted for 100% engrafted hNSC; in contrast, in mice treated with αC1q plus αC3a Abs, these markers accounted for only 84% engrafted hNSC. Mean ± SEM is shown. Scale bar, 25 μm.

data demonstrate novel alternative functions of both C1q and C3a on CNS cells.

C1q and C3a appear to account for the majority of fate- and migration-modulating activity in PMN-CM, because administration of blocking Abs returned hNSC astroglial differentiation to control levels and prevented ~76% of the hNSC chemotactic response. Surprisingly, a well-characterized TNF-α function-blocking Ab (30) had no effect, although TNF-α is not only produced by PMN, but has also been shown to mediate astroglial differentiation in vitro (39, 65, 66), and TNF-α–induced STAT3 signaling has been shown to be important for astroglial differentiation of neural progenitors (80, 81). These data could reflect a lack of

Table VII. CC3 analysis at 48 h in vitro

Condition	Number of $CC3^+$ Cells	*N*	Statistics
C1q at [PMN]	0.200 ± 0.891	4	NS
C1q at [Mϕ]	0.222 ± 0.084	4	NS
Control for C1q	0.139 ± 0.066	4	N/A
C3a at [PMN]	0.125 ± 0.063	4	Significant decrease compared with control; $p < 0.05$
C3a at [Mϕ]	0.308 ± 0.105	3	NS
Control for C3a	0.303 ± 0.072	7	N/A
C1q + C3a at [PMN]	0.322 ± 0.137	3	NS
C1q + C3a at [Mϕ]	0.234 ± 0.116	3	NS
Control for C1q + C3a	0.234 ± 0.116	3	N/A

N are indicated, and 10 random images were quantified per *N*. Mean ± SEM is shown. Statistical analyses were conducted using Student *t* test to compare with control for each condition. Significance is $p < 0.05$.

N/A, not applicable.

TNF-α receptor expression in this hNSC population, or developmental regulation of TNFR1/2 expression in neural stem versus progenitor cells (82). Future studies will further investigate the possible signaling mechanisms mediating the specific effect of complement-mediated astrogliogenesis in hNSC.

Addition of purified C1q plus C3a[PMN] to DM increased $GFAP^+$ cell fate and migration relative to DM control, as well as relative to C1q plus C3a[Mϕ]. However, the magnitude of this effect in response to purified C1q and C3a was less than that observed with CM. It is possible that purified C1q and C3a are less stable in vitro, and therefore exert a reduced biological effect. Alternatively, despite the lack of effect of αC1q and αC3a blocking Abs in DM control conditions and IgG control Abs in the presence of PMN-CM, we cannot exclude the possibility that αC1q and αC3a acted with other factors in PMN-CM to produce their effects. Ultimately, however, both blockade of complement proteins in PMN-CM and addition of purified ligands at PMN-synthesized concentration yield the same effect with respect to both astroglial differentiation and cell migration, highlighting a role for C1q and C3a in these processes.

We demonstrate significantly higher concentrations of Mϕ- versus PMN-derived C1q and C3a (a 14-fold and 6-fold difference, respectively). We also show that C1q plus C3a[Mϕ] did not alter the percentage of $GFAP^+$ cells compared with control. Furthermore, significantly fewer hNSC migrated toward this high concentration mixture of C1q and C3a compared with control, suggesting a repulsive effect. These data suggest that complement-mediated effects on fate and migration profiles of hNSC are concentration dependent. Although in some ways surprising, this observation is consistent with other literature in the field. For example, in vitro and in vivo studies have shown that increasing the concentration of SDF1α increases cell migration in a linear manner up to a saturation point, after which increasing concentration exerts a chemorepulsive effect (termed fugetaxis) (63, 64, 83, 84). Interestingly, monocytes secrete differential concentrations of both C1q and C3a proteins in an activation state–dependent manner (48, 49, 85, 86), suggesting there may be concentration-dependent physiological roles for these proteins. Identification and characterization of M1 versus M2 Mϕ subpopulations have recently come under fire (87–89), and discrimination between these two subtypes was not within the scope of the current study; however, we can speculate that, in parallel with differences between PMN and Mϕ C1q and C3a generation, variations in Mϕ activation state could also play a role in modulating neural stem and progenitor fate and migration. Moreover, the more complex inflammatory milieu in the developing, injured, or diseased CNS in vivo may further modulate neural stem and progenitor responses to these and other cues.

In the present experiments, hNSC fate profile was assessed in vitro using three principal markers of GFAP, β-tubulin III, and Olig2. Specifically, with respect to GFAP, previous studies have shown heterogeneity in both maturity and marker expression in cultures of human stem cell–derived astrocytes, but identify GFAP expression as a marker for astroglial identity (90), and GFAP is commonly used to characterize astroglial differentiation in hNSC cultures (91–93). Critically, more mature astroglial markers such as GLAST and ALDH1L1 are absent in human cell cultures <4 wk old (90). Additionally, our data are consistent with previous studies demonstrating the progressive loss of Nestin in NSC during differentiation in vitro, and the progressive upregulation of GFAP in a subpopulation of NSC that differentiate into astrocytes (94, 95).

In sum, we demonstrate a novel mechanism by which PMN and Mϕ modulate hNSC fate and migration. Although high concentrations of C3a have been previously shown to affect fate and migration of neural progenitors in the presence of SDF1α (78), our data identify complement proteins as a discrete mechanism by which PMN and Mϕ affect hNSC. Additionally, the current study suggests that this mechanism applies to a broader in vivo setting, in which endogenous and transplanted NSC are present in a microenvironment that contains inflammatory factors and/or cells, such as the developing, diseased, or injured CNS. In SCI, this inflammatory microenvironment has distinct temporal stages and a changing spatial distribution over the acute to chronic postinjury period (3–7). Accordingly, we suggest that understanding the cross-talk between transplanted cells and neuroinflammatory molecules may be critical for predicting the effects of local cues on donor cell properties, and for enhancing the repair or restoration of function by donor cells.

Acknowledgments

We thank Robert Tushinski and Dongping He at StemCells Inc. for technical support in maintenance of the human cells. We thank our undergraduates, Brian Ahn and Daniel Cantu, for contributions to immunostaining and quantification.

Disclosures

Nobuko Uchida has financial interest in StemCells Inc. The remaining authors have no financial conflicts of interest.

References

1. Shihabuddin, L. S., P. J. Horner, J. Ray, and F. H. Gage. 2000. Adult spinal cord stem cells generate neurons after transplantation in the adult dentate gyrus. *J. Neurosci.* 20: 8727–8735.
2. Wurmser, A. E., T. D. Palmer, and F. H. Gage. 2004. Neuroscience: cellular interactions in the stem cell niche. *Science* 304: 1253–1255.
3. Popovich, P. G., P. Wei, and B. T. Stokes. 1997. Cellular inflammatory response after spinal cord injury in Sprague-Dawley and Lewis rats. *J. Comp. Neurol.* 377: 443–464.

4. Kigerl, K. A., V. M. McGaughy, and P. G. Popovich. 2006. Comparative analysis of lesion development and intraspinal inflammation in four strains of mice following spinal contusion injury. *J. Comp. Neurol.* 494: 578–594.
5. Jones, T. B., E. E. McDaniel, and P. G. Popovich. 2005. Inflammatory-mediated injury and repair in the traumatically injured spinal cord. *Curr. Pharm. Des.* 11: 1223–1236.
6. Fleming, J. C., M. D. Norenberg, D. A. Ramsay, G. A. Dekaban, A. E. Marcillo, A. D. Saenz, M. Pasquale-Styles, W. D. Dietrich, and L. C. Weaver. 2006. The cellular inflammatory response in human spinal cords after injury. *Brain* 129: 3249–3269.
7. Beck, K. D., H. X. Nguyen, M. D. Galvan, D. L. Salazar, T. M. Woodruff, and A. J. Anderson. 2010. Quantitative analysis of cellular inflammation after traumatic spinal cord injury: evidence for a multiphasic inflammatory response in the acute to chronic environment. *Brain* 133: 433–447.
8. Zhang, R., Y. Liu, K. Yan, L. Chen, X. R. Chen, P. Li, F. F. Chen, and X. D. Jiang. 2013. Anti-inflammatory and immunomodulatory mechanisms of mesenchymal stem cell transplantation in experimental traumatic brain injury. *J. Neuroinflammation* 10: 106.
9. Butovsky, O., Y. Ziv, A. Schwartz, G. Landa, A. E. Talpalar, S. Pluchino, G. Martino, and M. Schwartz. 2006. Microglia activated by IL-4 or IFN-gamma differentially induce neurogenesis and oligodendrogenesis from adult stem/progenitor cells. *Mol. Cell. Neurosci.* 31: 149–160.
10. Pluchino, S., L. Zanotti, B. Rossi, E. Brambilla, L. Ottoboni, G. Salani, M. Martinello, A. Cattalini, A. Bergami, R. Furlan, et al. 2005. Neurosphere-derived multipotent precursors promote neuroprotection by an immunomodulatory mechanism. *Nature* 436: 266–271.
11. Javorkova, E., P. Trosan, A. Zajicova, M. Krulova, M. Hajkova, and V. Holan. 2014. Modulation of the early inflammatory microenvironment in the alkali-burned eye by systemically administered interferon-γ-treated mesenchymal stromal cells. *Stem Cells Dev.* 23: 2490–2500.
12. Tena, A., and D. H. Sachs. 2014. Stem cells: immunology and immunomodulation. *Dev. Ophthalmol.* 53: 122–132.
13. Ziv, Y., H. Avidan, S. Pluchino, G. Martino, and M. Schwartz. 2006. Synergy between immune cells and adult neural stem/progenitor cells promotes functional recovery from spinal cord injury. [Published erratum appears in 2006 *Proc. Natl. Acad. Sci. USA* 103: 18380.] *Proc. Natl. Acad. Sci. USA* 103: 13174–13179.
14. Soltys, J., J. Knight, E. Scharf, D. Pitt, and Y. Mao-Draayer. 2014. IFN-β alters neurotrophic factor expression in T cells isolated from multiple sclerosis patients: implication of novel neurotensin/NTSR1 pathway in neuroprotection. *Am. J. Transl. Res.* 6: 312–319.
15. Aarum, J., K. Sandberg, S. L. Haeberlein, and M. A. Persson. 2003. Migration and differentiation of neural precursor cells can be directed by microglia. *Proc. Natl. Acad. Sci. USA* 100: 15983–15988.
16. Nakanishi, M., T. Niidome, S. Matsuda, A. Akaike, T. Kihara, and H. Sugimoto. 2007. Microglia-derived interleukin-6 and leukemia inhibitory factor promote astrocytic differentiation of neural stem/progenitor cells. *Eur. J. Neurosci.* 25: 649–658.
17. Monje, M. L., H. Toda, and T. D. Palmer. 2003. Inflammatory blockade restores adult hippocampal neurogenesis. *Science* 302: 1760–1765.
18. Chen, Z., and T. D. Palmer. 2013. Differential roles of TNFR1 and TNFR2 signaling in adult hippocampal neurogenesis. *Brain Behav. Immun.* 30: 45–53.
19. Yoneyama, M., T. Shiba, S. Hasebe, and K. Ogita. 2011. Adult neurogenesis is regulated by endogenous factors produced during neurodegeneration. *J. Pharmacol. Sci.* 115: 425–432.
20. Moriyama, M., T. Fukuhara, M. Britschgi, Y. He, R. Narasimhan, S. Villeda, H. Molina, B. T. Huber, M. Holers, and T. Wyss-Coray. 2011. Complement receptor 2 is expressed in neural progenitor cells and regulates adult hippocampal neurogenesis. *J. Neurosci.* 31: 3981–3989.
21. Shinjyo, N., Y. de Pablo, M. Pekny, and M. Pekna. 2016. Complement peptide C3a promotes astrocyte survival in response to ischemic stress. *Mol. Neurobiol.* 53: 3076–3087.
22. Anderson, A. J., D. L. Haus, M. J. Hooshmand, H. Perez, C. J. Sontag, and B. J. Cummings. 2011. Achieving stable human stem cell engraftment and survival in the CNS: is the future of regenerative medicine immunodeficient? *Regen. Med.* 6: 367–406.
23. Luchetti, S., K. D. Beck, M. D. Galvan, R. Silva, B. J. Cummings, and A. Anderson. 2010. Comparison of immunopathology and locomotor recovery in C57BL/6, BUB/BnJ and NOD-scid mice after contusion spinal cord injury. *J. Neurotrauma* 27: 411–421.
24. Nguyen, H. X., T. J. O'Barr, and A. J. Anderson. 2007. Polymorphonuclear leukocytes promote neurotoxicity through release of matrix metalloproteinases, reactive oxygen species, and TNF-alpha. *J. Neurochem.* 102: 900–912.
25. Crowley, L. C., A. P. Scott, B. J. Marfell, J. A. Boughaba, G. Chojnowski, and N. J. Waterhouse. 2016. Measuring cell death by propidium iodide uptake and flow cytometry. *Cold Spring Harb. Protoc.* 2016: pdb prot087163.
26. Uchida, N., D. W. Buck, D. He, M. J. Reitsma, M. Masek, T. V. Phan, A. S. Tsukamoto, F. H. Gage, and I. L. Weissman. 2000. Direct isolation of human central nervous system stem cells. *Proc. Natl. Acad. Sci. USA* 97: 14720–14725.
27. Tamaki, S., K. Eckert, D. He, R. Sutton, M. Doshe, G. Jain, R. Tushinski, M. Reitsma, B. Harris, A. Tsukamoto, et al. 2002. Engraftment of sorted/expanded human central nervous system stem cells from fetal brain. *J. Neurosci. Res.* 69: 976–986.
28. Piltti, K. M., D. L. Haus, E. Do, H. Perez, A. J. Anderson, and B. J. Cummings. 2011. Computer-aided 2D and 3D quantification of human stem cell fate from in vitro samples using Volocity high performance image analysis software. *Stem Cell Res. (Amst.)* 7: 256–263.
29. Burger, R., A. Bader, M. Kirschfink, U. Rother, L. Schrod, I. Wörner, and G. Zilow. 1987. Functional analysis and quantification of the complement C3 derived anaphylatoxin C3a with a monoclonal antibody. *Clin. Exp. Immunol.* 68: 703–711.
30. Selmaj, K. W., M. Farooq, W. T. Norton, C. S. Raine, and C. F. Brosnan. 1990. Proliferation of astrocytes in vitro in response to cytokines: a primary role for tumor necrosis factor. *J. Immunol.* 144: 129–135.
31. Zgraggen, S., R. Huggenberger, K. Kerl, and M. Detmar. 2014. An important role of the SDF-1/CXCR4 axis in chronic skin inflammation. *PLoS One* 9: e93665.
32. Vaithilingam, A., J. E. Teixeira, P. J. Miller, B. T. Heron, and C. D. Huston. 2012. *Entamoeba histolytica* cell surface calreticulin binds human c1q and functions in amebic phagocytosis of host cells. *Infect. Immun.* 80: 2008–2018.
33. Hooshmand, M. J., C. J. Sontag, N. Uchida, S. Tamaki, A. J. Anderson, and B. J. Cummings. 2009. Analysis of host-mediated repair mechanisms after human CNS-stem cell transplantation for spinal cord injury: correlation of engraftment with recovery. *PLoS One* 4: e5871.
34. Cummings, B. J., N. Uchida, S. J. Tamaki, D. L. Salazar, M. Hooshmand, R. Summers, F. H. Gage, and A. J. Anderson. 2005. Human neural stem cells differentiate and promote locomotor recovery in spinal cord-injured mice. *Proc. Natl. Acad. Sci. USA* 102: 14069–14074.
35. Anderson, A. J., J. H. Su, and C. W. Cotman. 1996. DNA damage and apoptosis in Alzheimer's disease: colocalization with c-Jun immunoreactivity, relationship to brain area, and effect of postmortem delay. *J. Neurosci.* 16: 1710–1719.
36. Sontag, C. J., N. Uchida, B. J. Cummings, and A. J. Anderson. 2014. Injury to the spinal cord niche alters the engraftment dynamics of human neural stem cells. *Stem Cell Rep.* 2: 620–632.
37. Joelving, F. C., R. Billeskov, J. R. Christensen, M. West, and B. Pakkenberg. 2006. Hippocampal neuron and glial cell numbers in Parkinson's disease: a stereological study. *Hippocampus* 16: 826–833.
38. Politis, P. K., D. Thomaidou, and R. Matsas. 2008. Coordination of cell cycle exit and differentiation of neuronal progenitors. *Cell Cycle* 7: 691–697.
39. Ben-Hur, T., O. Ben-Menachem, V. Furer, O. Einstein, R. Mizrachi-Kol, and N. Grigoriadis. 2003. Effects of proinflammatory cytokines on the growth, fate, and motility of multipotential neural precursor cells. *Mol. Cell. Neurosci.* 24: 623–631.
40. Zhang, C., S. Jang, O. C. Amadi, K. Shimizu, R. T. Lee, and R. N. Mitchell. 2013. A sensitive chemotaxis assay using a novel microfluidic device. *BioMed Res. Int.* 2013: 373569.
41. Imitola, J., K. Raddassi, K. I. Park, F. J. Mueller, M. Nieto, Y. D. Teng, D. Frenkel, J. Li, R. L. Sidman, C. A. Walsh, et al. 2004. Directed migration of neural stem cells to sites of CNS injury by the stromal cell-derived factor 1alpha/CXC chemokine receptor 4 pathway. *Proc. Natl. Acad. Sci. USA* 101: 18117–18122.
42. Lewellis, S. W., and H. Knaut. 2012. Attractive guidance: how the chemokine SDF1/CXCL12 guides different cells to different locations. *Semin. Cell Dev. Biol.* 23: 333–340.
43. Bleul, C. C., R. C. Fuhlbrigge, J. M. Casasnovas, A. Aiuti, and T. A. Springer. 1996. A highly efficacious lymphocyte chemoattractant, stromal cell-derived factor 1 (SDF-1). *J. Exp. Med.* 184: 1101–1109.
44. Kokovay, E., S. Goderie, Y. Wang, S. Lotz, G. Lin, Y. Sun, B. Roysam, Q. Shen, and S. Temple. 2010. Adult SVZ lineage cells home to and leave the vascular niche via differential responses to SDF1/CXCR4 signaling. *Cell Stem Cell* 7: 163–173.
45. Lacy, P., and J. L. Stow. 2011. Cytokine release from innate immune cells: association with diverse membrane trafficking pathways. *Blood* 118: 9–18.
46. Rot, A., and U. H. von Andrian. 2004. Chemokines in innate and adaptive host defense: basic chemokinese grammar for immune cells. *Annu. Rev. Immunol.* 22: 891–928.
47. Nguyen, H. X., M. D. Galvan, and A. J. Anderson. 2008. Characterization of early and terminal complement proteins associated with polymorphonuclear leukocytes in vitro and in vivo after spinal cord injury. *J. Neuroinflammation* 5: 26.
48. Taylor-Robinson, D., H. U. Schorlemmer, P. M. Furr, and A. C. Allison. 1978. Macrophage secretion and the complement cleavage product C3a in the pathogenesis of infections by mycoplasmas and L-forms of bacteria and in immunity to these organisms. *Clin. Exp. Immunol.* 33: 486–494.
49. Zhou, A. Q., M. J. Herriott, and R. W. Leu. 1991. Kinetics of the biosynthesis of complement subcomponent C1q by murine macrophages: LPS, immune complexes, and zymosan alone and in combination with interferon-gamma. *J. Leukoc. Biol.* 50: 453–463.
50. Camous, L., L. Roumenina, S. Bigot, S. Brachemi, V. Frémeaux-Bacchi, P. Lesavre, and L. Halbwachs-Mecarelli. 2011. Complement alternative pathway acts as a positive feedback amplification of neutrophil activation. *Blood* 117: 1340–1349.
51. Okuda, T. 1991. Murine polymorphonuclear leukocytes synthesize and secrete the third component and factor B of complement. *Int. Immunol.* 3: 293–296.
52. Rahpeymai, Y., M. A. Hietala, U. Wilhelmsson, A. Fotheringham, I. Davies, A. K. Nilsson, J. Zwirner, R. A. Wetsel, C. Gerard, M. Pekny, and M. Pekna. 2006. Complement: a novel factor in basal and ischemia-induced neurogenesis. *EMBO J.* 25: 1364–1374.
53. Botto, M., D. Lissandrini, C. Sorio, and M. J. Walport. 1992. Biosynthesis and secretion of complement component (C3) by activated human polymorphonuclear leukocytes. *J. Immunol.* 149: 1348–1355.

54. Bentley, C., W. Fries, and V. Brade. 1978. Synthesis of factors D, B and P of the alternative pathway of complement activation, as well as of C3, by guinea-pig peritoneal macrophages in vitro. *Immunology* 35: 971–980.
55. Bexborn, F., P. O. Andersson, H. Chen, B. Nilsson, and K. N. Ekdahl. 2008. The tick-over theory revisited: formation and regulation of the soluble alternative complement C3 convertase (C3(H2O)Bb). *Mol. Immunol.* 45: 2370–2379.
56. Wirthmueller, U., B. Dewald, M. Thelen, M. K. Schäfer, C. Stover, K. Whaley, J. North, P. Eggleton, K. B. Reid, and W. J. Schwaeble. 1997. Properdin, a positive regulator of complement activation, is released from secondary granules of stimulated peripheral blood neutrophils. *J. Immunol.* 158: 4444–4451.
57. Zewde, N., R. D. Gorham, Jr., A. Dorado, and D. Morikis. 2016. Quantitative modeling of the alternative pathway of the complement system. *PLoS One* 11: e0152337.
58. Schwartz, L. B., M. S. Kawahara, T. E. Hugli, D. Vik, D. T. Fearon, and K. F. Austen. 1983. Generation of C3a anaphylatoxin from human C3 by human mast cell tryptase. *J. Immunol.* 130: 1891–1895.
59. Yuan, X., M. Shan, R. You, M. V. Frazier, M. J. Hong, R. A. Wetsel, S. Drouin, A. Seryshev, L. Z. Song, L. Cornwell, et al. 2015. Activation of C3a receptor is required in cigarette smoke-mediated emphysema. *Mucosal Immunol.* 8: 874–885.
60. Johnson, U., K. Ohlsson, and I. Olsson. 1976. Effects of granulocyte neutral proteases on complement components. *Scand. J. Immunol.* 5: 421–426.
61. Venge, P., and I. Olsson. 1975. Cationic proteins of human granulocytes. VI. Effects on the complement system and mediation of chemotactic activity. *J. Immunol.* 115: 1505–1508.
62. Des Prez, R. M., C. S. Bryan, J. Hawiger, and D. G. Colley. 1975. Function of the classical and alternate pathways of human complement in serum treated with ethylene glycol tetraacetic acid and MgCl2-ethylene glycol tetraacetic acid. *Infect. Immun.* 11: 1235–1243.
63. Tharp, W. G., R. Yadav, D. Irimia, A. Upadhyaya, A. Samadani, O. Hurtado, S. Y. Liu, S. Munisamy, D. M. Brainard, M. J. Mahon, et al. 2006. Neutrophil chemorepulsion in defined interleukin-8 gradients in vitro and in vivo. *J. Leukoc. Biol.* 79: 539–554.
64. Vianello, F., N. Papeta, T. Chen, P. Kraft, N. White, W. K. Hart, M. F. Kircher, E. Swart, S. Rhee, G. Palù, et al. 2006. Murine B16 melanomas expressing high levels of the chemokine stromal-derived factor-1/CXCL12 induce tumor-specific T cell chemorepulsion and escape from immune control. *J. Immunol.* 176: 2902–2914.
65. Ricci-Vitiani, L., P. Casalbore, G. Petrucci, L. Lauretti, N. Montano, L. M. Larocca, M. L. Falchetti, D. G. Lombardi, V. D. Gerevini, C. Cenciarelli, et al. 2006. Influence of local environment on the differentiation of neural stem cells engrafted onto the injured spinal cord. *Neurol. Res.* 28: 488–492.
66. Johansson, S., J. Price, and M. Modo. 2008. Effect of inflammatory cytokines on major histocompatibility complex expression and differentiation of human neural stem/progenitor cells. *Stem Cells* 26: 2444–2454.
67. Salazar, D. L., N. Uchida, F. P. Hamers, B. J. Cummings, and A. J. Anderson. 2010. Human neural stem cells differentiate and promote locomotor recovery in an early chronic spinal cord injury NOD-scid mouse model. *PLoS One* 5: e12272.
68. Nguyen, H., M. H. H. Saiwai, J. Maddox, A. Salehi, D. Salazar, N. Uchida, and A. Anderson. Systemic neutrophil depletion modulates the migration and fate of transplanted human neural stem cells to rescue functional repair. *J. Neurosci.* In press.
69. Benoit, M. E., and A. J. Tenner. 2011. Complement protein C1q-mediated neuroprotection is correlated with regulation of neuronal gene and microRNA expression. *J. Neurosci.* 31: 3459–3469.
70. Reboul, A., M. H. Prandini, J. C. Bensa, and M. G. Colomb. 1985. Characterization of C1q, C1s and C-1 Inh synthesized by stimulated human monocytes in vitro. *FEBS Lett.* 190: 65–68.
71. Bensa, J. C., A. Reboul, and M. G. Colomb. 1983. Biosynthesis in vitro of complement subcomponents C1q, C1s and C1 inhibitor by resting and stimulated human monocytes. *Biochem. J.* 216: 385–392.
72. Arnett, H. A., Y. Wang, G. K. Matsushima, K. Suzuki, and J. P. Ting. 2003. Functional genomic analysis of remyelination reveals importance of inflammation in oligodendrocyte regeneration. *J. Neurosci.* 23: 9824–9832.
73. Anderson, A. J., S. Robert, W. Huang, W. Young, and C. W. Cotman. 2004. Activation of complement pathways after contusion-induced spinal cord injury. *J. Neurotrauma* 21: 1831–1846.
74. Stephan, A. H., D. V. Madison, J. M. Mateos, D. A. Fraser, E. A. Lovelett, L. Coutellier, L. Kim, H. H. Tsai, E. J. Huang, D. H. Rowitch, et al. 2013. A dramatic increase of C1q protein in the CNS during normal aging. *J. Neurosci.* 33: 13460–13474.
75. Stevens, B., N. J. Allen, L. E. Vazquez, G. R. Howell, K. S. Christopherson, N. Nouri, K. D. Micheva, A. K. Mehalow, A. D. Huberman, B. Stafford, et al. 2007. The classical complement cascade mediates CNS synapse elimination. *Cell* 131: 1164–1178.
76. Tahtouh, M., F. Croq, J. Vizioli, P. E. Sautiere, C. Van Camp, M. Salzet, M. R. Daha, J. Pestel, and C. Lefebvre. 2009. Evidence for a novel chemotactic C1q domain-containing factor in the leech nerve cord. *Mol. Immunol.* 46: 523–531.
77. Bogestål, Y. R., S. R. Barnum, P. L. Smith, V. Mattisson, M. Pekny, and M. Pekna. 2007. Signaling through C5aR is not involved in basal neurogenesis. *J. Neurosci. Res.* 85: 2892–2897.
78. Shinjyo, N., A. Ståhlberg, M. Dragunow, M. Pekny, and M. Pekna. 2009. Complement-derived anaphylatoxin C3a regulates in vitro differentiation and migration of neural progenitor cells. *Stem Cells* 27: 2824–2832.
79. Johswich, K., and A. Klos. 2007. C5L2: an anti-inflammatory molecule or a receptor for acylation stimulating protein (C3a-desArg)? *Adv. Exp. Med. Biol.* 598: 159–180.
80. Chen, E., D. Xu, X. Lan, B. Jia, L. Sun, J. C. Zheng, and H. Peng. 2013. A novel role of the STAT3 pathway in brain inflammation-induced human neural progenitor cell differentiation. *Curr. Mol. Med.* 13: 1474–1484.
81. Sofroniew, M. V. 2015. Astrocyte barriers to neurotoxic inflammation. *Nat. Rev. Neurosci.* 16: 249–263.
82. Carpentier, P. A., and T. D. Palmer. 2009. Immune influence on adult neural stem cell regulation and function. *Neuron* 64: 79–92.
83. Alsayed, Y., H. Ngo, J. Runnels, X. Leleu, U. K. Singha, C. M. Pitsillides, J. A. Spencer, T. Kimlinger, J. M. Ghobrial, X. Jia, et al. 2007. Mechanisms of regulation of CXCR4/SDF-1 (CXCL12)-dependent migration and homing in multiple myeloma. *Blood* 109: 2708–2717.
84. Vianello, F., I. T. Olszak, and M. C. Poznansky. 2005. Fugetaxis: active movement of leukocytes away from a chemokinetic agent. *J. Mol. Med. (Berl.)* 83: 752–763.
85. Tenner, A. J., and D. B. Volkin. 1986. Complement subcomponent C1q secreted by cultured human monocytes has subunit structure identical with that of serum C1q. *Biochem. J.* 233: 451–458.
86. Ferluga, J., H. U. Schorlemmer, L. C. Baptista, and A. C. Allison. 1978. Production of the complement cleavage product, C3a, by activated macrophages and its tumorolytic effects. *Clin. Exp. Immunol.* 31: 512–517.
87. Kigerl, K. A., J. C. Gensel, D. P. Ankeny, J. K. Alexander, D. J. Donnelly, and P. G. Popovich. 2009. Identification of two distinct macrophage subsets with divergent effects causing either neurotoxicity or regeneration in the injured mouse spinal cord. *J. Neurosci.* 29: 13435–13444.
88. Mantovani, A., A. Sica, S. Sozzani, P. Allavena, A. Vecchi, and M. Locati. 2004. The chemokine system in diverse forms of macrophage activation and polarization. *Trends Immunol.* 25: 677–686.
89. Heppner, F. L., R. M. Ransohoff, and B. Becher. 2015. Immune attack: the role of inflammation in Alzheimer disease. *Nat. Rev. Neurosci.* 16: 358–372.
90. Roybon, L., N. J. Lamas, A. Garcia-Diaz, E. J. Yang, R. Sattler, V. Jackson-Lewis, Y. A. Kim, C. A. Kachel, J. D. Rothstein, S. Przedborski, et al. 2013. Human stem cell-derived spinal cord astrocytes with defined mature or reactive phenotypes. *Cell Reports* 4: 1035–1048.
91. Shaltouki, A., J. Peng, Q. Liu, M. S. Rao, and X. Zeng. 2013. Efficient generation of astrocytes from human pluripotent stem cells in defined conditions. *Stem Cells* 31: 941–952.
92. Haas, C., and I. Fischer. 2013. Human astrocytes derived from glial restricted progenitors support regeneration of the injured spinal cord. *J. Neurotrauma* 30: 1035–1052.
93. Corti, S., M. Nizzardo, C. Simone, M. Falcone, C. Donadoni, S. Salani, F. Rizzo, M. Nardini, G. Riboldi, F. Magri, et al. 2012. Direct reprogramming of human astrocytes into neural stem cells and neurons. *Exp. Cell Res.* 318: 1528–1541.
94. Schneider, L., S. Pellegatta, R. Favaro, F. Pisati, P. Roncaglia, G. Testa, S. K. Nicolis, G. Finocchiaro, and F. d'Adda di Fagagna. 2013. DNA damage in mammalian neural stem cells leads to astrocytic differentiation mediated by BMP2 signaling through JAK-STAT. *Stem Cell Rep.* 1: 123–138.
95. Obayashi, S., H. Tabunoki, S. U. Kim, and J. Satoh. 2009. Gene expression profiling of human neural progenitor cells following the serum-induced astrocyte differentiation. *Cell. Mol. Neurobiol.* 29: 423–438.